Covariant Local Matrix Density Approximation through Spectral Reconstruction in Multistate Density Functional Theory

Alexander Humeniuk,[*,†] Yangyi Lu,[*,‡] and Jiali Gao[‡,¶,§]

†*independent researcher*

‡*Institute of Systems and Physical Biology, Shenzhen Bay Laboratory, Shenzhen 518055, China*

¶*School of Chemical Biology and Biotechnology, Beijing University Shenzhen Graduate School, Shenzhen 518055, China*

§*Department of Chemistry and Supercomputing Institute, University of Minnesota, Minneapolis, Minnesota 55455, United States*

E-mail: alexander.humeniuk@gmail.com; luyy@szbl.ac.cn

Abstract

A covariant local matrix density approximation (LMDA) is introduced within multistate density functional theory based on subspace invariance and the spectral decomposition of the matrix containing state and transition densities. The exchange-correlation matrix functional is constructed through spectral reconstruction of this matrix density, whereby conventional local exchange-correlation functionals are incorporated as spectral-channel functionals within a covariant matrix-functional formalism. The resulting formulation preserves exact normalization of the exchange-correlation matrix hole, recovers Kohn-Sham density functional theory in the single-state limit, and preserves spin-multiplet degeneracy through covariance of the spin matrix functional under spin rotations. Combined with multistate self-consistent-field (MSSCF) optimization, the present framework enables fully variational calculations of interacting ground and excited states. Applications to atomic excitations, H_2 dissociation, ethylene torsion and cyclobutadiene automerization reveals that the resulting MSDFT/LMDA approach captures essential multistate and strong-correlation physics, including static correlation and spin symmetry. The key insight is that the central obstacle in extending density functional theory to coupled electronic states is not necessarily the lack of appropriate scalar exchange-correlation approximations, but the lack of a covariant matrix-functional formalism in which such functionals can operate. The present MSDFT/LMDA provides a direct realization of this matrix-functional formalism.

TOC Graphic

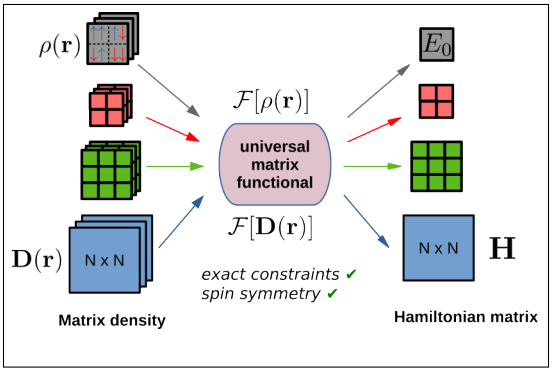

Keywords

Local matrix-density approximation, Exchange matrix hole, Covariant matrix functional, Strong correlation, Multistate density functional theory, Spin-Multiplet Degeneracy

1 Introduction

Kohn–Sham density functional theory (KS-DFT) has become one of the most broadly successful methods for electronic-structure calculations because it combines predictive accuracy with computational efficiency.[1–6] Its success is driven largely by the systematic development of exchange–correlation approximations over the past four decades, which have established a hierarchy of methods for ground-state properties.[7–13] Extending this level of reliability to excited states, however, remains a major challenge. Linear-response time-dependent DFT (LR-TDDFT) is widely used and often provides accurate excitation energies for weakly correlated systems,[14–17] but it is known to fail in situations involving strong correlation and multiconfigurational character, including double excitations, near degeneracies, conical intersections, open-shell systems, and bond dissociation.[18–21] Despite extensive developments of variational, state-weighting, and state-specific excited-state DFT formulations,[22–30] a unified density-functional method capable of treating strongly interacting electronic states is still elusive, reflecting fundamental limitations of scalar-density descriptions for multistate systems.[31] In the present work, we show that a covariant multistate matrix functional can be generated directly from the spectral decomposition of the matrix density using local, scalar exchange-correlation functionals developed for KS-DFT, enabling a fully self-consistent treatment of multistate electronic structure and strong correlation.

Multistate density functional theory (MSDFT) addresses the challenge of coupled electronic states by promoting the fundamental variable from a scalar density to a matrix density that contains both state and transition densities.[32–34] Within an N-dimensional Hilbert subspace, the matrix density $\mathbf{D}(\mathbf{r})$ determines the projected Hamiltonian through a covariant matrix functional $\mathcal{H}[\mathbf{D}]$, while the physical states are obtained variationally from the trace of the Hamiltonian matrix functional. By treating state densities and transition densities altogether, MSDFT naturally incorporates electronic coherence, state coupling, and multiconfigurational character within a unified variational formalism.

Recent developments have established both the formal foundation and practical represen-

tations needed to make MSDFT computationally tractable.[34–36] In particular, the minimal active space (MAS) representation of the matrix density[33] and the nonorthogonal state interaction (NOSI) formalism[37] provide efficient strategies for constructing interacting-state subspaces. In previous applications, however, the Hamiltonian matrix functional has generally been approximated element by element, using KS-DFT exchange-correlation functionals for diagonal matrix elements together with physically motivated models for off-diagonal couplings.[37–46] Although successful in many applications, particularly in regimes where KS-DFT and LR-TDDFT encounter difficulties, this strategy does not provide a unified exchange-correlation matrix functional and does not automatically preserve the covariance and subspace invariance required for a true matrix-density functional theory.

A fundamentally different perspective emerges from recent formal analysis showing that the Hamiltonian is a covariant matrix functional of the matrix density whose structure is independent of the dimension of the Hilbert subspace.[35] Under unitary transformations within the subspace, the matrix density and Hamiltonian transform covariantly, ensuring that observable quantities remain invariant with respect to the representation of the interacting states.[36,47] Consequently, the ground-state ($N = 1$) and multistate ($N > 1$) cases should be viewed as different realizations of the same functional object, with the additional complexity arising primarily from the noncommutativity of matrix operations.[35] These covariance (equivalently, subspace-invariance) conditions impose fundamental constraints on admissible matrix functionals and provide the formal foundation for extending density functional theory to interacting electronic states.[35,36]

For local functionals there is a close connection to the theory of analytic matrix functions, according to which a single scalar function in the spectral representation of $\mathbf{D}(\mathbf{r})$ uniquely determines the full matrix function.[36,47] Within this formalism, the matrix density is locally diagonalized into eigendensities and spectral projectors, the scalar function of the local exchange-correlation energy density is evaluated for the eigendensity channels, and the matrix functional is reconstructed covariantly through the same projector basis. As a

result, off-diagonal matrix elements emerge naturally from the same underlying scalar functional rather than requiring independent approximations.[35,36] The central challenge therefore shifts from modeling individual matrix elements to constructing practical matrix functionals that preserve unitary covariance and subspace invariance. These developments motivate the central objective of the present work: the construction of a practical local matrix density approximation (LMDA) within a fully self-consistent multistate SCF formalism.

This study contains three principal advances: (i) a covariant spectral construction of matrix exchange-correlation functionals, (ii) the first fully variational implementation of a local matrix-density approximation within multistate DFT, and (iii) a spin-covariant matrix-functional formulation that preserves spin-multiplet degeneracy. In the following, we first summarize the formal foundations of MSDFT and introduce the exchange-correlation (xc) matrix hole, which is the generalization of the xc hole to multiple states. We then present the spin-resolved matrix formalism together with the multistate self-consistent-field (MSSCF) optimization procedure. Finally, applications to atomic excitations, H_2 dissociation, ethylene torsion and cyclobutadiene automerization demonstrate that the MSDFT/LMDA approach captures essential multistate and strong-correlation physics.

2 Background

2.1 Essentials of MSDFT

The nonrelativistic electronic Hamiltonian of an n-electron system is denoted by $\hat{H}$. We define the matrix density $\mathbf{D}(\mathbf{r})$ corresponding to N orthonormal many-electron states $\{\Psi_I, I = 1, \cdots, N\}$ with elements[48]

$$D_{IJ}(\mathbf{r}) = \langle \Psi_I | \hat{\rho}(\mathbf{r}) | \Psi_J \rangle, \tag{1}$$

where $\hat{\rho}(\mathbf{r})$ is the electronic density operator.

MSDFT establishes that, within the N-dimensional Hilbert subspace spanned by $\{\Psi_I\}$,

there exists a one-to-one correspondence between the matrix density $\mathbf{D}(\mathbf{r})$ and the Hamiltonian matrix.[32] Consequently, the Hamiltonian matrix can be expressed as a matrix functional of the matrix density,

$$\mathcal{H}[\mathbf{D}] = \mathcal{F}[\mathbf{D}] + \int v(\mathbf{r})\mathbf{D}(\mathbf{r})\mathrm{d}\mathbf{r} \tag{2}$$

where $\mathcal{F}[\mathbf{D}]$ is a universal matrix functional, independent of the external potential $v(\mathbf{r})$.[34] Furthermore, variational minimization of the trace of $\mathcal{H}[\mathbf{D}]$ yields the exact matrix density of the subspace $\mathbb{S}^N$ spanned by the lowest N eigenstates,[31,32,34]

$$\mathbb{E}[\mathbf{D}] = \min_{\mathbf{D}(\mathbf{r})} \frac{1}{N} \mathrm{tr}\left(\mathcal{H}[\mathbf{D}]\right). \tag{3}$$

Then, diagonalization of the Hamiltonian matrix functional constructed from the optimized matrix density yields the N eigenenergies $\{\mathrm{E}_I; I = 1, \cdots, N\}$ of the subspace.

2.2 Subspace Invariance and Covariance of the Hamiltonian Matrix Functional

A fundamental requirement of MSDFT is that physical observables be independent of the representation within the Hilbert subspace $\mathbb{S}^N$. Since different sets of basis states spanning the same subspace are related by unitary transformations, the matrix density transforms as

$$\mathbf{D}'(\mathbf{r}) = \mathbf{U}\mathbf{D}(\mathbf{r})\mathbf{U}^\dagger, \tag{4}$$

where $\mathbf{U}$ is an arbitrary N-dimensional unitary matrix independent of $\mathbf{r}$. Unitary invariance of the Hilbert subspace therefore requires the Hamiltonian matrix functional to transform covariantly,

$$\mathcal{H}[\mathbf{D}'] = \mathbf{U}\mathcal{H}[\mathbf{D}]\mathbf{U}^\dagger. \tag{5}$$

This covariance condition guarantees that observable quantities, including energies and degeneracies, remain invariant under basis rotations within the subspace and therefore constitutes a fundamental exact condition constraining admissible matrix functionals.[36,47] In particular, the Hamiltonian matrix functional cannot be approximated element by element, since independent approximations for individual matrix elements do not in general preserve subspace invariance under unitary transformations.[35]

Throughout this article, *covariance* denotes the transformation law of matrix functionals under unitary rotations within the Hilbert subspace, while *subspace invariance* refers to the resulting invariance of physical observables. *Spin-rotation invariance* denotes the corresponding covariance under SU(2) spin rotations, which preserves spin-multiplet degeneracy.

2.3 Hamiltonian Matrix Functional

The electronic Hamiltonian consists of the kinetic-energy, electron–electron interaction, and external-potential operators. Accordingly, the Hamiltonian matrix functional $\mathcal{H}[\mathbf{D}]$ may be decomposed as

$$\mathcal{H}[\mathbf{D}] = \mathbf{T}[\mathbf{D}] + \mathbf{E}^{\mathrm{H}}[\mathbf{D}] + \mathbf{E}^{\mathrm{xc}}[\mathbf{D}] + \int v(\mathbf{r})\mathbf{D}(\mathbf{r})\mathrm{d}\mathbf{r} \tag{6}$$

where $\mathbf{T}[\mathbf{D}]$, $\mathbf{E}^{\mathrm{H}}[\mathbf{D}]$ and $\mathbf{E}^{\mathrm{xc}}[\mathbf{D}]$ denote the kinetic, Hartree, and exchange–correlation matrix functionals, respectively.

In principle, the kinetic-energy matrix is also an exact matrix functional of $\mathbf{D}(\mathbf{r})$. In practice, however, accurate orbital-free kinetic-energy functionals remain unavailable even for conventional ground-state DFT. In the present work, the kinetic-energy matrix is therefore evaluated explicitly from auxiliary multiconfigurational wave functions that parametrize the matrix density,[33]

$$T_{AB}[\mathbf{D}] = \langle \Phi_A^{\mathrm{MS}} | \hat{T} | \Phi_B^{\mathrm{MS}} \rangle. \tag{7}$$

Here, the auxiliary multistate wave functions $\{\Phi_A^{\mathrm{MS}}\}$ are represented using complete-active-space-type expansions, as described below.

The external-potential contribution is linear in the matrix density,

$$V_{AB}[\mathbf{D}] = \int v(\mathbf{r}) D_{AB}(\mathbf{r}) d\mathbf{r}. \tag{8}$$

Consequently, the external potential contributes not only to diagonal matrix elements through state densities ($A = B$), but also to off-diagonal couplings through transition densities.

The Hartree matrix functional provides the simplest nontrivial example of how covariance modifies the structure of multistate energy functionals. In order to satisfy the unitary-covariance condition of eq 5, the Hartree contribution must be constructed as a matrix product of matrix densities at positions $\mathbf{r}$ and $\mathbf{r}'$,[35]

$$E^{\mathrm{H}}_{AB}[\mathbf{D}] = \frac{1}{2} \sum_{C=1}^{N} \iint \frac{D_{AC}(\mathbf{r}) D_{CB}(\mathbf{r}')}{|\mathbf{r} - \mathbf{r}'|} \, d\mathbf{r} \, d\mathbf{r}'. \tag{9}$$

Thus, even the Coulomb interaction is no longer determined solely by the diagonal state densities, but also contains contributions from transition densities through intermediate-state couplings. The multistate Hartree functional therefore depends intrinsically on the matrix structure of the density.

The exchange-correlation contribution is defined through the universal matrix functional as $\mathbf{E}^{\mathrm{xc}}[\mathbf{D}] = \mathcal{F}[\mathbf{D}] - \mathbf{T}[\mathbf{D}] - \mathbf{E}^{\mathrm{H}}[\mathbf{D}]$, which may further be partitioned into exchange and correlation contributions, $\mathbf{E}^{\mathrm{xc}}[\mathbf{D}] = \mathbf{X}[\mathbf{D}] + \mathbf{C}[\mathbf{D}]$. Conventional local exchange and correlation functionals of KS-DFT are turned into covariant matrix functionals through spectral reconstruction of the matrix density (*vide infra*), with KS-DFT recovered in the single-state limit ($N = 1$).

3 Theory

In this section, we extend the exchange-correlation (xc) hole formalism of KS-DFT to MS-DFT. We first introduce the pair matrix density and define the multistate xc hole together

with its exact normalization condition. We then show that covariance gives rise to a spectral representation of the matrix hole.

3.1 Exchange Matrix Holes

3.1.1 Ground-State Exchange Hole and the Homogeneous Electron Gas

The exchange hole plays a central role in the construction of modern exchange-correlation functionals in KS-DFT.[49–52] It describes the reduction in electronic probability surrounding a reference electron arising from antisymmetry and Coulomb correlation.[3,5,52–54] Expressing the exchange-correlation energy as the Coulomb interaction between an electron and its associated hole yields important exact constraints, including hole normalization, correct short-range behavior, and recovery of the homogeneous electron gas (HEG) limit.

For the HEG, the exchange hole is[53]

$$h_{\uparrow}^{x,\mathrm{HEG}}(u) = -9\rho_{\uparrow}\left(\frac{j_1(k_F u)}{k_F u}\right)^2, \tag{10}$$

where $k_F = (6\pi^2\rho_{\uparrow})^{1/3}$ is the Fermi momentum and $j_1(x) = \sin(x)/x^2 - \cos(x)/x$ is the first-order spherical Bessel function. In LDA, this expression is applied locally using the density at each spatial position.

3.1.2 Pair Matrix Density and the Exchange-Correlation Matrix Hole

To generalize the exchange-hole formalism to interacting electronic states, it is convenient to start with the pair-electron matrix density $\mathbf{D}^{(2e)}(\mathbf{r},\mathbf{r}')$ within the subspace $\mathbb{S}^N$,

$$\begin{aligned} D_{IJ}^{(2e)}(\mathbf{r},\mathbf{r}') = n(n-1) \sum_{\sigma_1,\sigma_2,\ldots,\sigma_n} \int \mathrm{d}\mathbf{r}_3 \ldots \int \mathrm{d}\mathbf{r}_n \\ \Psi_I(\mathbf{r}\sigma_1,\mathbf{r}'\sigma_2,\mathbf{r}_3\sigma_3,\ldots,\mathbf{r}_n\sigma_n)\Psi_J^*(\mathbf{r}\sigma_1,\mathbf{r}'\sigma_2,\mathbf{r}_3\sigma_3,\ldots,\mathbf{r}_n\sigma_n) \end{aligned} \tag{11}$$

which reduces to the conventional ground-state pair density for $N = 1$.[55]

The exchange-correlation matrix hole is defined through

$$D_{IJ}^{(2e)}(\mathbf{r},\mathbf{r}') := \sum_K D_{IK}(\mathbf{r})\{D_{KJ}(\mathbf{r}') + H_{KJ}^{\mathrm{xc}}(\mathbf{r},\mathbf{r}')\}. \tag{12}$$

or, equivalently,

$$\mathbf{H}^{\mathrm{xc}}(\mathbf{r},\mathbf{r}') = \mathbf{D}^{-1}(\mathbf{r})\mathbf{D}^{(2e)}(\mathbf{r},\mathbf{r}') - \mathbf{D}(\mathbf{r}') \tag{13}$$

This definition immediately yields the exact matrix-hole normalization condition (Appendices A and B),

$$\int \mathbf{H}^{\mathrm{xc}}(\mathbf{r},\mathbf{r}')\mathrm{d}\mathbf{r}' = -\mathbf{I} \tag{14}$$

which applies simultaneously to both diagonal and off-diagonal matrix elements.

The exchange-correlation matrix functional is then expressed as the Coulomb interaction between the matrix density and the matrix hole,

$$E_{IJ}^{\mathrm{xc}}[\mathbf{D}] = \frac{1}{2}\int \mathrm{d}\mathbf{r} \sum_K D_{IK}(\mathbf{r}) \int \mathrm{d}\mathbf{r}' \frac{H_{KJ}^{\mathrm{xc}}(\mathbf{r},\mathbf{r}')}{|\mathbf{r}-\mathbf{r}'|}. \tag{15}$$

3.1.3 Covariant Spectral Reconstruction

At each spatial position $\mathbf{r}$, e.g., a numerical grid point, $\mathbf{D}(\mathbf{r})$ can be expressed as the spectral decomposition[36]

$$\mathbf{D}(\mathbf{r}) = \sum_i \lambda_i(\mathbf{r})\mathbf{P}_i(\mathbf{r}) \tag{16}$$

where $\lambda_i(\mathbf{r})$ and $\mathbf{P}_i(\mathbf{r})$ are the eigendensities and spectral projectors of the matrix density, respectively. For nondegenerate eigenvalues, $\mathbf{P}_i = |u_i(\mathbf{r})\rangle\langle u_i(\mathbf{r})|$, where $|u_i(\mathbf{r})\rangle$ is the eigenvector associated with $\lambda_i(\mathbf{r})$.

Within the local density approximation, exchange holes may be evaluated independently for each spectral channel and subsequently recombined through the projectors to yield the

full covariant matrix exchange hole,

$$\mathbf{H}^{x}(\mathbf{r},\mathbf{r}') = \sum_i h^{x,\mathrm{HEG}}\big(\lambda_i(\mathbf{r}); u\big)\, \mathbf{P}_i(\mathbf{r}), \qquad u = |\mathbf{r}-\mathbf{r}'|. \tag{17}$$

3.2 Local Matrix Density Approximation

The LMDA follows directly from the spectral structure of analytic matrix functions. At each spatial position $\mathbf{r}$, the matrix density is resolved into local spectral channels through its eigendensities $\{\lambda_i\}$ and projectors $\{\mathbf{P}_i\}$, while unitary-matrix covariance and subspace invariance are restored through spectral recomposition.[36] The exchange-correlation matrix functional is therefore expressed as

$$\mathbf{E}_{\mathrm{xc}}^{\mathrm{LMDA}}[\mathbf{D}] = \int d\mathbf{r}\, \mathcal{E}_{\mathrm{xc}}^{\mathrm{LMDA}}(\mathbf{D}(\mathbf{r})), \tag{18}$$

with the *exchange-correlation matrix density* given by

$$\mathcal{E}_{\mathrm{xc}}^{\mathrm{LMDA}}(\mathbf{D}(\mathbf{r})) = \sum_i \epsilon_{\mathrm{xc}}^{\mathrm{LDA}}(\lambda_i(\mathbf{r}))\mathbf{P}_i(\mathbf{r}), \tag{19}$$

where $\lambda_i(\mathbf{r})$ and $\mathbf{P}_i(\mathbf{r})$ are the eigendensities and spectral projectors of $\mathbf{D}(\mathbf{r})$, respectively (eq 16). Equation (19) embeds the conventional local KS-DFT exchange-correlation functional into a covariant matrix-functional construction that preserves subspace invariance while reducing to KS-DFT in the single-state limit ($N = 1$).

The scalar exchange contribution to ϵ_{xc} is represented by the Dirac local-density form,[3,56]

$$\epsilon_x^{\mathrm{D}}(\rho) = -C_x\rho^{4/3}, \qquad C_x = \frac{3}{4}\left(\frac{6}{\pi}\right)^{1/3},$$

while correlation is described using the Chachiyo parameterization of the quantum Monte

Carlo data on uniform electron gas,[57,58]

$$\epsilon_c^{\mathrm{CCA}}(\rho) = a \log\left(1 + b_1\rho^{1/3} + b_2\rho^{2/3}\right)\rho \tag{20}$$

with parameters given in Reference 57. Equation (20) employs spin-averaged eigendensities for the scalar exchange–correlation channels. Extension to spin-dependent matrix densities requires covariance to be preserved consistently with spin-rotation symmetry and spin-multiplet degeneracy, as discussed in the following subsection.

3.3 Spin-Invariant Matrix Functional

In conventional scalar-density formulations, the open-shell singlet and the $M_S = 0$ triplet possess identical charge densities and therefore cannot be distinguished without introducing spin-polarized densities. However, spin-polarized functionals generally break spin symmetry and lift the degeneracy of spin multiplets.[59] In MSDFT, by contrast, electronic states are characterized not only by their state densities but also by their transition densities within the multistate subspace. Consequently, states with identical charge densities may still possess distinct matrix-density structure and different energies, while spin-multiplet degeneracy is preserved through covariance of the matrix functional rather than through explicit spin polarization of the scalar density (Fig. 1).

Spin rotations are represented by unitary transformations $\mathbf{U}_{\mathrm{spin}} \in \mathrm{SU}(2)$,

$$\mathbf{U}_{\mathrm{spin}}(\gamma, \hat{n}) = \exp\left(-i\frac{\gamma}{2}\left[n_x\sigma_x + n_y\sigma_y + n_z\sigma_z\right]\right) \tag{21}$$

where γ is the rotation angle around the axis $\hat{n} = (n_x, n_y, n_z)$ and $\sigma_x, \sigma_y, \sigma_z$ are the Pauli matrices. Within an N-state subspace $\mathbb{S}^N$, the spin-resolved matrix density is represented

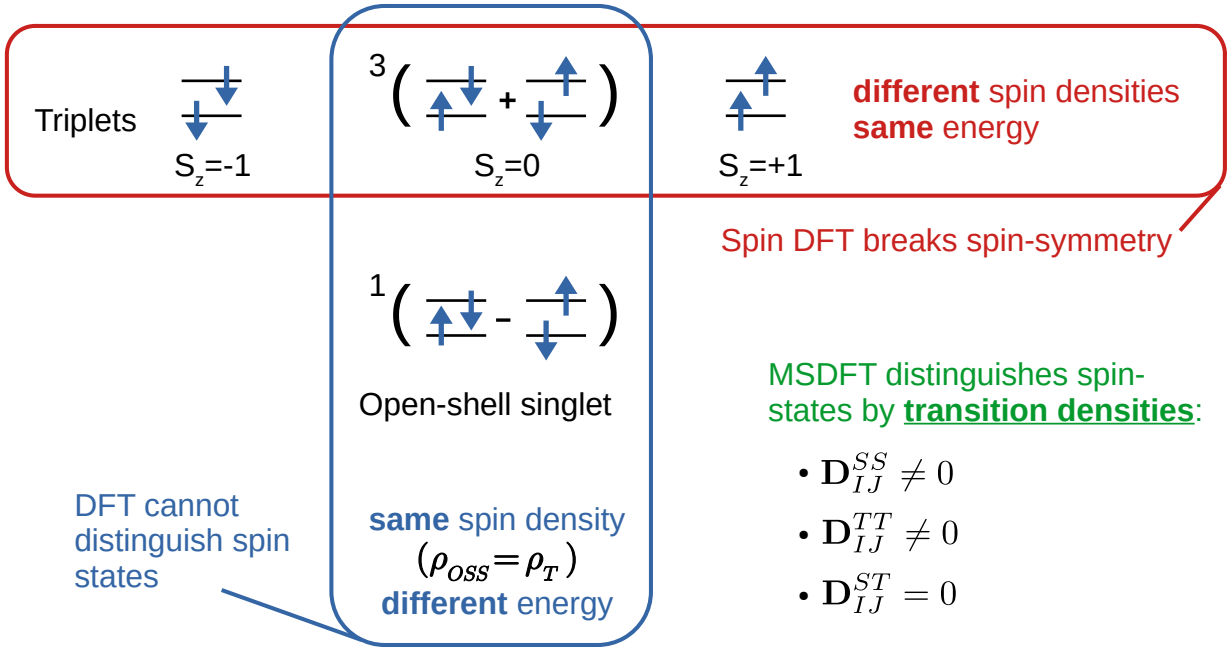

Figure 1: MSDFT resolves the spin dilemma by distinguishing spin states through their transition densities within the multistate subspace. The open-shell singlet and the $M_S = 0$ triplet possess identical charge densities but different transition-density structure and therefore different energies, while triplet components with different spin densities remain exactly degenerate under spin rotations.

by the $2N \times 2N$ spin matrix density

$$\tilde{\mathbf{D}}(\mathbf{r}) = \begin{pmatrix} \mathbf{D}^{\alpha\alpha}(\mathbf{r}) & \mathbf{D}^{\alpha\beta}(\mathbf{r}) \\ \mathbf{D}^{\beta\alpha}(\mathbf{r}) & \mathbf{D}^{\beta\beta}(\mathbf{r}) \end{pmatrix}, \tag{22}$$

with matrix elements

$$\tilde{D}^{\sigma\sigma'}_{IJ}(\mathbf{r}) = \langle \Psi_I | \hat{\rho}_{\sigma\sigma'}(\mathbf{r}) | \Psi_J \rangle, \qquad \sigma, \sigma' = \alpha, \beta. \tag{23}$$

The spin-summed charge matrix density is recovered through

$$\mathbf{D}(\mathbf{r}) = \mathrm{Tr}_{\mathrm{spin}} \tilde{\mathbf{D}}(\mathbf{r}). \tag{24}$$

Under spin rotations, the spin matrix density transforms covariantly,

$$\tilde{\mathbf{D}}'(\mathbf{r}) = \mathbf{U}_{\mathrm{spin}}\tilde{\mathbf{D}}(\mathbf{r})\mathbf{U}_{\mathrm{spin}}^{\dagger}. \tag{25}$$

Because spin rotations mix diagonal and off-diagonal spin blocks, a functional depending only on $\mathbf{D}^{\alpha\alpha}$ and $\mathbf{D}^{\beta\beta}$ is not closed under the transformation. Spin-rotational invariance therefore requires the Hamiltonian matrix functional to depend on the full spin matrix density, including the mixed-spin blocks $\mathbf{D}^{\alpha\beta}$ and $\mathbf{D}^{\beta\alpha}$.

The spin-covariant extension enlarges the matrix representation from the N-dimensional subspace density to the full $2N$-dimensional spin matrix density while preserving the underlying scalar spectral-channel structure. Consequently, the spin matrix functional is reconstructed from the same nonzero eigendensity channels associated with the multistate subspace, whereas covariance under spin rotations is carried by the spectral projectors of the enlarged spin matrix density.

We therefore introduce a local analytic matrix function $\mathbf{G}(\tilde{\mathbf{D}}(\mathbf{r}))$ and define the spin-invariant matrix functional as

$$\mathcal{G}[\tilde{\mathbf{D}}] = \int d\mathbf{r}\, \mathrm{Tr}_{\mathrm{spin}}\left[\mathbf{G}(\tilde{\mathbf{D}}(\mathbf{r}))\right]. \tag{26}$$

Covariance under spin rotations requires

$$\mathbf{G}(\mathbf{U}_{\mathrm{spin}}\tilde{\mathbf{D}}(\mathbf{r})\mathbf{U}_{\mathrm{spin}}^{\dagger}) = \mathbf{U}_{\mathrm{spin}}\mathbf{G}(\tilde{\mathbf{D}}(\mathbf{r}))\mathbf{U}_{\mathrm{spin}}^{\dagger}, \tag{27}$$

and the cyclic invariance of the spin trace immediately yields

$$\mathcal{G}[\tilde{\mathbf{D}}'] = \mathcal{G}[\tilde{\mathbf{D}}] \tag{28}$$

demonstrating invariance under spin rotations. Spin symmetry is not restored through ex-

ternal constraints or symmetry projection, but instead emerges naturally from covariance of the matrix functional itself.

4 Method and Computational Details

4.1 Variational Optimization of the Matrix Density

In the present implementation, the matrix density itself is treated as the fundamental variational object, while the exchange-correlation matrix functional is evaluated through covariant spectral reconstruction of local scalar channels. The overall computational workflow of MSDFT with the local matrix density approximation (LMDA) is summarized in Fig. 2. The variational parameters consist of the antisymmetric orbital-rotation matrix $\mathbf{R}_{\mathrm{MO}}$ and the state-rotation matrix $\mathbf{R}_{\mathrm{CI}}$, which together determine the rank-N matrix density $\mathbf{D}(\mathbf{r})$. Gradients are evaluated by backpropagation through the full computational graph, including construction of the matrix density, spectral decomposition, numerical integration of the matrix functional, and evaluation of the variational objective.

The subspace energy $\mathbb{E}[\mathbf{D}]$ of eq 3 is minimized self-consistently with respect to the orbital and state-rotation parameters. When degenerate states are present, all components of the degenerate manifold must be included in the subspace trace. After convergence, the adiabatic state energies are obtained by diagonalization of the Hamiltonian matrix functional evaluated at the variational minimum.[32]

4.2 Spin-Resolved Matrix Functional

Different spin treatments correspond to different covariant representations of the spin matrix density. In the present work, the scalar channel function in eq 19 was evaluated using four different spin representations.

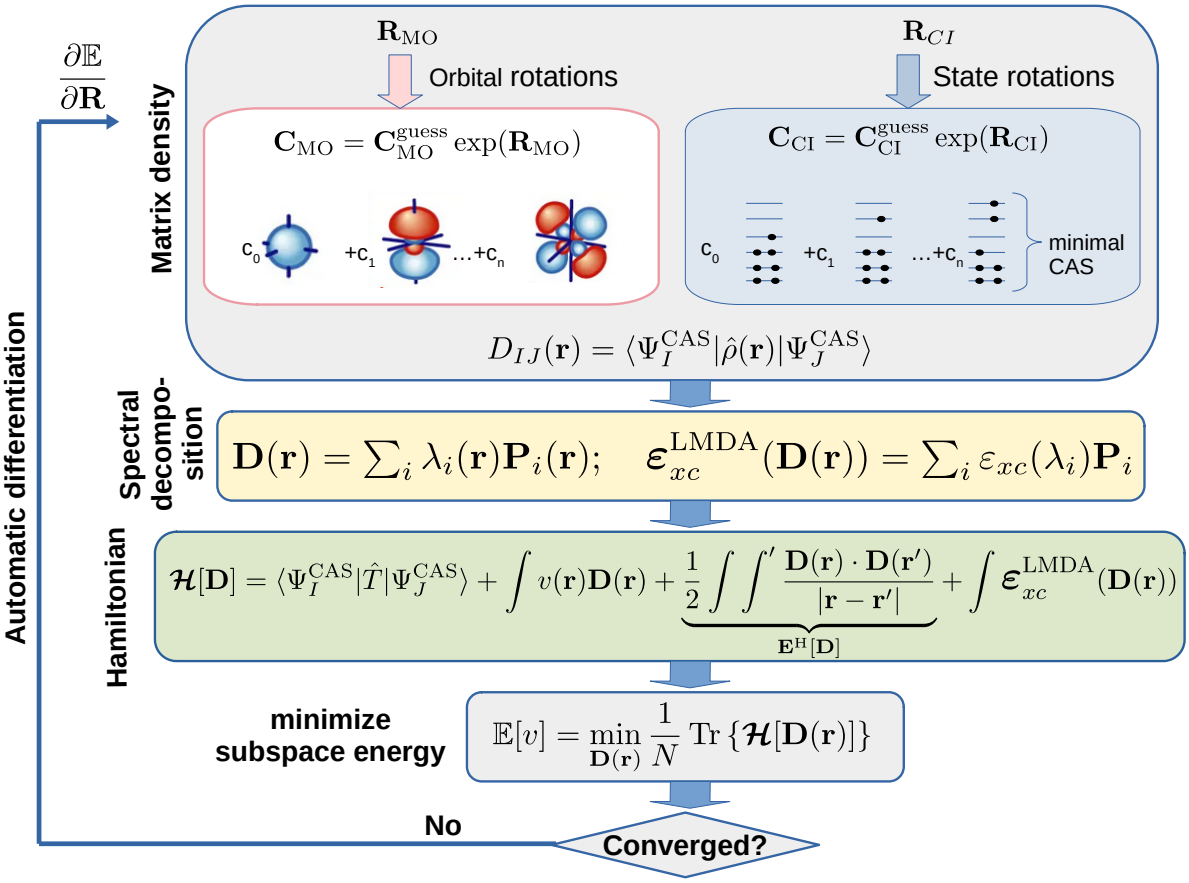

Figure 2: Variational optimization of the MSDFT subspace energy. Orbital and state rotations determine the matrix density, from which the Hamiltonian matrix functional is evaluated. Gradients are obtained by automatic differentiation through the matrix-functional computational graph.

4.2.1 Spin-Invariant Representation

The spin density is represented by the full $(2N) \times (2N)$ spin matrix density $\tilde{\mathbf{D}}(\mathbf{r})$, containing the $\alpha\alpha$, $\beta\beta$, and mixed-spin $\alpha\beta/\beta\alpha$ blocks. Spectral decomposition is therefore performed in the complete spinor space, yielding $2N$ local eigendensities (see Appendix C). The exchange matrix functional is then obtained by tracing over the spin degrees of freedom,

$$\epsilon_x^{\mathrm{inv}}(\tilde{\mathbf{D}}(\mathbf{r})) = \mathrm{Tr}_{\mathrm{spin}} \left[\mathbf{G} \left(\tilde{\mathbf{D}}(\mathbf{r}) \right) \right]. \tag{29}$$

Because the functional transforms covariantly under arbitrary unitary transformations in the full spinor space, this representation preserves spin-rotational invariance and exact spin-multiplet degeneracy.

4.2.2 Spin-Polarized Representation

The spin-polarized matrix density retains only the diagonal spin blocks, $\mathbf{D}^{\alpha\alpha}$ and $\mathbf{D}^{\beta\beta}$, while neglecting the mixed-spin components. The exchange matrix functional is evaluated independently in the α and β spin sectors,

$$\epsilon_x^{\mathrm{pol}}(\tilde{\mathbf{D}}(\mathbf{r})) = \mathbf{G}(\mathbf{D}^{\alpha\alpha}(\mathbf{r})) + \mathbf{G}(\mathbf{D}^{\beta\beta}(\mathbf{r})). \tag{30}$$

This representation breaks spin-rotational invariance because the exchange matrix functional depends explicitly on the spin polarization of the density. In the present calculations, only the $S_z = 0$ sector was included, consisting of the open-shell singlet and the ${}^3(\uparrow\downarrow)$ triplet component, since couplings between states with different S_z vanish identically within this representation. To account for the missing multiplet components the state energies were weighted by their multiplicities $2S + 1$.

4.2.3 Spin-Unpolarized Representation

In the spin-unpolarized formulation, the total density is used as the scalar input for the spectral channels,

$$\epsilon_x^{\mathrm{unpol}}(\mathbf{D}(\mathbf{r})) = 2\mathbf{G}\left[\frac{1}{2}\left(\mathbf{D}^{\alpha\alpha}(\mathbf{r}) + \mathbf{D}^{\beta\beta}(\mathbf{r})\right)\right]. \tag{31}$$

This representation preserves rotational invariance but removes the distinction between spin-coupled singlet and triplet states because they possess the same total density.

4.2.4 Equal-Weight Admixture

Finally, an equal-weight admixture of the invariant and spin-unpolarized exchange matrix functionals was examined,

$$\epsilon_x^{\mathrm{mix}}(\tilde{\mathbf{D}}(\mathbf{r})) = \frac{1}{2}\epsilon_x^{\mathrm{inv}}(\tilde{\mathbf{D}}(\mathbf{r})) + \frac{1}{2}\epsilon_x^{\mathrm{unpol}}(\mathbf{D}(\mathbf{r})). \tag{32}$$

Both contributions preserve unitary covariance and spin-multiplet degeneracy, while the mixed representation partially suppresses the excessive spin-coupling stabilization present in the fully invariant form.

The final exchange matrix functional is obtained by integration of the local exchange matrix density over all space,

$$\mathbf{X}[\tilde{\mathbf{D}}] = \int d\mathbf{r}\ \epsilon_x^{\mathrm{D}}(\tilde{\mathbf{D}}(\mathbf{r})). \tag{33}$$

In all calculations, the correlation matrix functional is evaluated from the spin-traced charge matrix density, $\mathbf{D}(\mathbf{r})$ as

$$\mathbf{C}[\mathbf{D}] = \int d\mathbf{r}\ \epsilon_c^{\mathrm{CCA}}(\mathbf{D}). \tag{34}$$

4.3 Numerical Implementation

The self-consistent optimization of the MSDFT subspace energy was implemented using *PyTorch* modules.[60] Derivatives of the multistate energy with respect to the variational parameters defining the matrix density were evaluated through automatic differentiation, enabling gradient-based quasi-Newton minimization. Because differentiation through analytic matrix functions is less straightforward than for scalar functionals, the details of the chain rule and backpropagation for matrix functions are provided in Appendices D and E.

To represent the $N \times N$-dimensional matrix density, we employ N auxiliary state functions

constructed in a complete-active-space (CAS) representation with n_{cas} active electrons in m orthonormal orbitals. These CAS wavefunctions serve a similar purpose as the Kohn-Sham determinant: They are used for evaluating the kinetic energy and to parameterize the matrix density from which all other parts of the Hamiltonian matrix can be calculated.

The active orbitals are expanded in atomic orbitals represented with the cc-pVDZ basis set. PySCF was used to evaluate electronic integrals, generate numerical integration grids, and construct the matrix density from the CAS auxiliary wavefunctions.[61] Because PySCF typically operates within a fixed value of S_z using separate α and β electron strings,[62,63] additional routines were implemented to construct the mixed-spin blocks $\mathbf{D}^{\alpha\beta}$ and $\mathbf{D}^{\beta\alpha}$ required for spin-covariant matrix functionals.

For numerical stability, matrix functionals were evaluated only at grid points where the average subspace density exceeded the Libxc threshold of 10^{-15}.[64] In the single-state limit, $N = 1$, the present multistate matrix functionals reduce exactly to their corresponding scalar KS-DFT functionals.

4.4 Computational Details

All MSDFT calculations employed the default numerical integration grids implemented in PySCF.[61] The LMDA was realized through covariant spectral reconstruction, effectively corresponding to N local KS-DFT-like channel evaluations together with diagonalization of the N-dimensional matrix density at each grid point. Dirac exchange and the Chachiyo-Ceperley-Alder correlation functional were used with the spectral channel eigendensities.

Unless otherwise stated, the cc-pVDZ basis set was employed. The basis is sufficient for the present proof-of-principle investigation of covariant matrix functionals and enables direct comparison with FCI calculations.

4.4.1 Atomic Spectra

MSDFT and FCI calculations were carried out for low-lying atomic states of H through O. The aug-cc-pVDZ basis set was used for H and He, while cc-pVDZ was employed for the remaining atoms.

The matrix densities were constructed using minimal active spaces consisting of the $2s$ and $2p$ orbitals for all atoms, with the $1s$ orbital also included for H and He. Initial orbitals for MSDFT calculations were obtained from diagonalization of the core Hamiltonian, whereas FCI calculations employed Hartree–Fock references corresponding to spherically symmetric closed-shell configurations. A gradient threshold of 10^{-5} was used for both orbital and configuration optimizations, and the BFGS algorithm was employed throughout. Adiabatic energies were obtained by diagonalization of the Hamiltonian matrix constructed from the optimized matrix densities.

4.4.2 H_2 Dissociation and Ethylene Torsion

Both MSDFT and wavefunction calculations employed minimal two-electron/two-orbital active spaces formed from the σ_g/σ_u orbitals of H_2 and the π/π^* orbitals of ethylene using the cc-pVDZ basis set.

The rigid torsional scan of ethylene employed the geometry $r(\mathrm{CC}) = 1.330$ Å, $r(\mathrm{CH}) = 1.076$ Å, and $\angle(\mathrm{HCH}) = 116.6°$, taken from Krylov and Sherrill.[65] In MSDFT, the subspace energy was minimized self-consistently with respect to both orbital and configuration coefficients. FCI and XMS-CASPT2 calculations were carried out using PySCF and BAGEL, respectively.[66,67]

4.4.3 Cyclobutadiene

The active space consists of four electrons in the four π_z orbitals. Since no attempt was made to optimize or reduce the active-space representation, the brute-force CAS expansion is rather large. Consequently, the matrix density was constructed from ROHF/cc-pVDZ orbitals and

the MSDFT Hamiltonian was diagonalized only once, an MS-CAS-CI alternative, to obtain the state energies.

The intermediate geometries in the scan were interpolated linearly in internal coordinates between the rectangular minimum (r(C=C) = 1.367 $\AA$, r(C-C) = 1.573 $\AA$, r(C-H) = 1.093 $\AA$, $\angle$(HCC)= 134.9°) and the square transition state (r(C-C) = 1.461 $\AA$, r(C-H) = 1.092 $\AA$, $\angle$(HCC)= 135°).[68] The MR-AQCC/SA-4-CASSCF/cc-pVTZ reference energies were digitized from Figure 2 of Reference 68.

5 Results

The following calculations examine whether essential multistate and strong-correlation physics can emerge from a local exchange-correlation functional once it is incorporated within a covariant matrix-functional formalism.

5.1 Exchange-Correlation Matrix Hole

Figure 3 (and Fig. S1) compare the "exact" exchange-correlation (xc) matrix holes of the ^3P, ^1D, and ^1S states of the carbon atom, obtained from FCI pair densities through eq 13, with the corresponding matrix holes determined by MSDFT using the LMDA and the Taylor expansion of the HEG exchange hole (Apendix B). All nine degenerate components of the three atomic terms are included (but only the ^3P states are shown in Fig. 3). The spherically averaged xc holes are shown as functions of the interelectronic separation $u = |\mathbf{r}' - \mathbf{r}_0|$ for reference points located at the nucleus and at $z = 0.2a_0$, respectively, in Fig. 3(a,b) and Fig. 3(c,d).

The diagonal xc holes are nearly indistinguishable across all states, indicating that the short-range exchange structure is remarkably similar among the ^3P, ^1D, and ^1S manifolds. In contrast, the off-diagonal elements exhibit greater variation, reflecting differences in interstate coupling encoded in the transition densities.

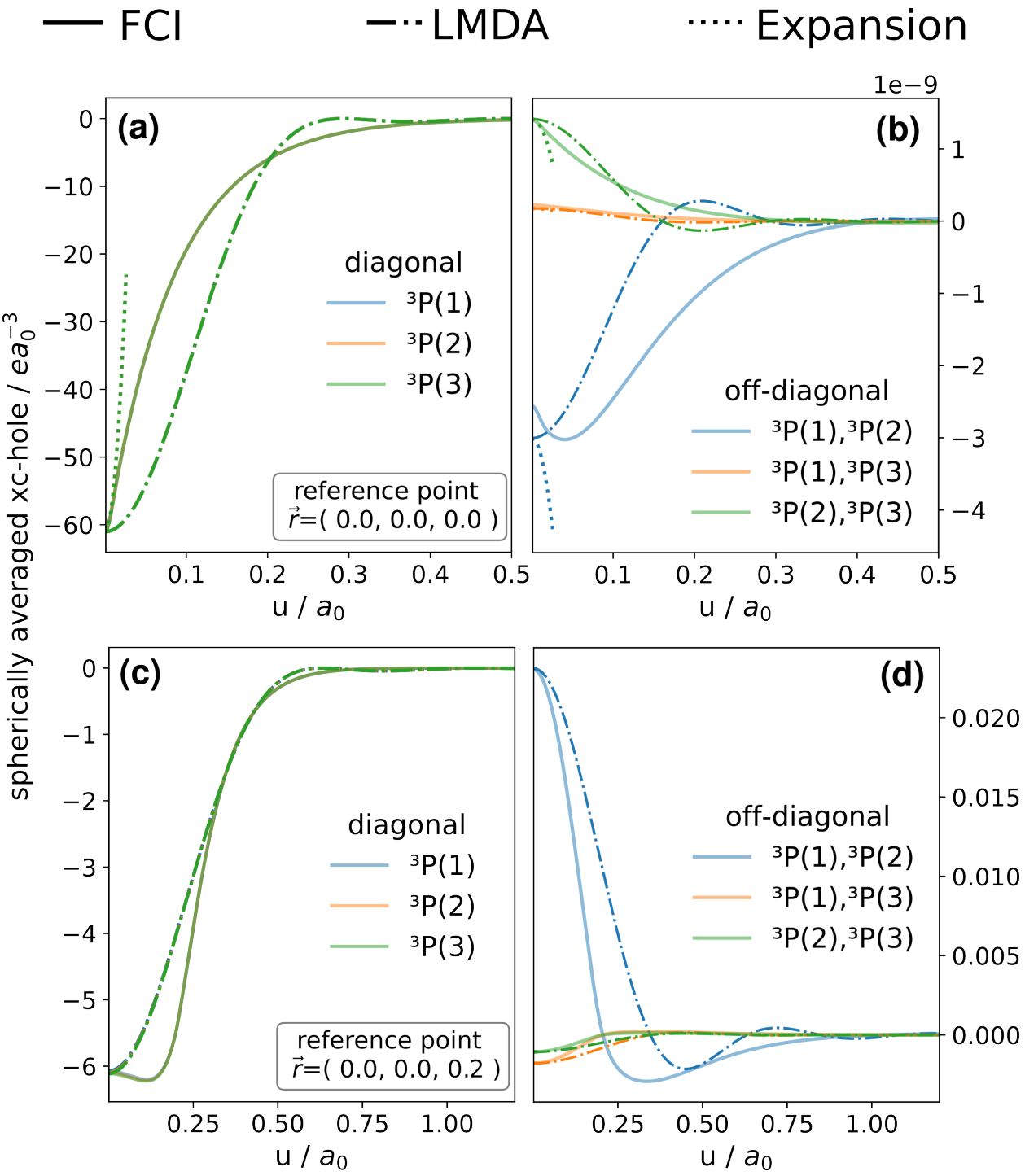

Figure 3: Diagonal (a,c) and off-diagonal (b,d) elements of spherically averaged exchange-correlation hole (solid) of the lowest triplet subspace (^3P) of carbon and the approximate LMDA exchange hole (dash-dotted) and its Taylor expansion (dotted), around the nucleus (top row) and around $z = 0.2a_0$ (bottom row). The xc-hole of the full low-energy subspace spanned by the lowest ^1S, ^3P and ^1D states is shown in the SI.

Because the ^3P and ^1D manifolds are respectively degenerate, the corresponding matrix densities are defined only up to unitary rotations within each degenerate subspace. Consequently, individual off-diagonal elements of the xc hole depend on the chosen representation of the degenerate states. Nevertheless, the xc hole is a subspace-invariant matrix function, and therefore such variations correspond only to unitary rotations that leave the overall error relative to the exact hole unchanged.

The HEG-based LMDA hole (dash-dotted lines in Fig. 3) qualitatively reproduces both diagonal and off-diagonal features of the exact FCI xc hole, despite the absence of explicit correlation effects. The short-range Taylor expansion accurately captures the behavior near $u = 0$ for the nucleus-centered reference point of Fig. 3(a,b), but deviations increase rapidly with interelectronic separation. For the displaced reference point in Fig. 3(c,d), however, the Taylor expansion remains in reasonable agreement with the FCI results.

Finally, numerical integration of the spherically averaged exchange (or exchange-correlation) holes yields values close to -1 for the diagonal elements and zero for the off-diagonal elements, consistent with the exact normalization conditions.

5.2 Spin-Resolved MSDFT

Figure 1 illustrates a minimal local spectral model for analyzing spin matrix density in MSDFT. For the two-electron-two-orbital system, the spin matrix density associated with the HOMO-LUMO manifold (eq C38) is completely characterized by the local spectral polarization, which allows analytical expressions for the LMDA exchange functional to be derived (Appendix C). The parameter

$$\xi(\mathbf{r}) = \frac{|\phi_H(\mathbf{r})|^2 - |\phi_L(\mathbf{r})|^2}{|\phi_H(\mathbf{r})|^2 + |\phi_L(\mathbf{r})|^2} \tag{35}$$

varies from -1, corresponding to pure local LUMO character, to $+1$, corresponding to pure local HOMO character, with $\xi = 0$ representing equal local contributions from the two

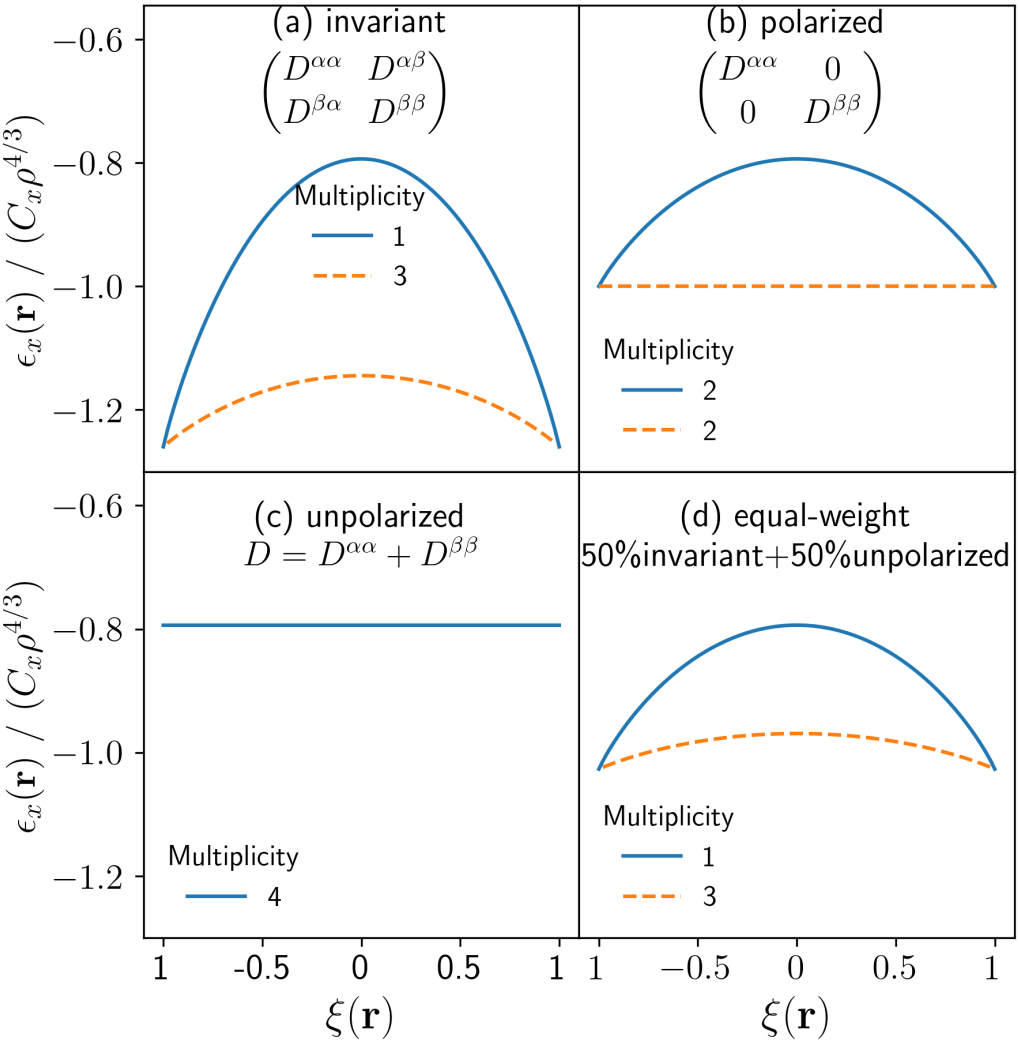

Figure 4: Eigenvalues of the exchange-energy matrix functional, $\boldsymbol{\epsilon}_x(\mathbf{D}(\mathbf{r}))$, as functions of the local spectral polarization $\xi(\mathbf{r})$ at spatial position $\mathbf{r}$ for the subspace consisting of the open-shell singlet state $\Psi_{S,0}$ and the triplet states $\Psi_{T,-1}$, $\Psi_{T,0}$, and $\Psi_{T,+1}$. All eigenvalues are reported in units of $C_x\rho^{4/3}$. Panel (a) shows results obtained using the spin-rotation-invariant matrix density $\tilde{\mathbf{D}}$, for which the three triplet states remain exactly degenerate (brown dashed curves). Panel (b) presents results from the spin-polarized matrix density, yielding two doubly degenerate pairs of eigenvalues. Panel (c) shows the results obtained using the total matrix density $\mathbf{D}$, for which all four states become indistinguishable. Panel (d) illustrates the equal-weight admixture of the two spin-rotation-invariant constructions, defined as $\boldsymbol{\epsilon}_x^{\mathrm{mix}} = \{\boldsymbol{\epsilon}_x^{\mathrm{inv}}(\tilde{\mathbf{D}}) + \boldsymbol{\epsilon}_x^{\mathrm{tot}}(\mathbf{D})\}/2$ which interpolates between the polarized and unpolarized descriptions while preserving spin-rotation invariance.

orbitals.

Figure 4 shows the eigenvalues of the exchange energy density at a spatial point $\mathbf{r}$ as functions of the spectral polarization ξ for different spin-density representations considered in MSDFT (section 4.2). Several important observations emerge from these results.

(a) The spin-rotation-invariant formulation preserves the exact triplet-multiplet degeneracy and reproduces the correct singlet-triplet splitting pattern, Fig. 4(a). The off-diagonal spin blocks are therefore essential for recovering the proper spin-covariant structure of the exchange matrix functional. However, incorporating coherent spin mixing among the triplet components also produces a systematic lowering of the exchange energies relative to the spin-polarized representation.

(b) Neglecting the off-diagonal spin-coherence blocks $\mathbf{D}^{\alpha\beta}$ and $\mathbf{D}^{\beta\alpha}$ reduces the matrix density to the conventional collinear spin-density form used in standard KS-DFT. The resulting exchange functional is no longer invariant under spin rotation, producing an unphysical splitting of the triplet manifold in Fig. 4(b). In particular, the open-shell singlet and the $M_S = 0$ triplet state become spuriously degenerate,

$$E_x^{\mathrm{pol}}({}^3(\uparrow\uparrow)) = E_x^{\mathrm{pol}}({}^3(\downarrow\downarrow)) \neq E_x^{\mathrm{pol}}({}^3(\uparrow\downarrow)) = E_x^{\mathrm{pol}}({}^1(\uparrow\downarrow)). \tag{36}$$

(c) In the spin-unpolarized formulation, the spin-traced matrix density $\mathbf{D}$ serves as the sole input variable to the exchange functional, analogous to the spin-restricted approximation in KS-DFT. Consequently, the exchange functional cannot distinguish among the triplet components and the open-shell singlet state (Fig. 4(c)).

(d) We further constructed an equal-weight admixture of the spin-rotation-invariant and spin-unpolarized exchange functionals, thereby incorporating both coherent spin coupling and spin-independent exchange contributions. As shown in Fig. 4(d), this mixed representation preserves spin symmetry while retaining the ability to distinguish states of different spin multiplicities, yielding exchange energies similar to those of the spin-polarized representation.

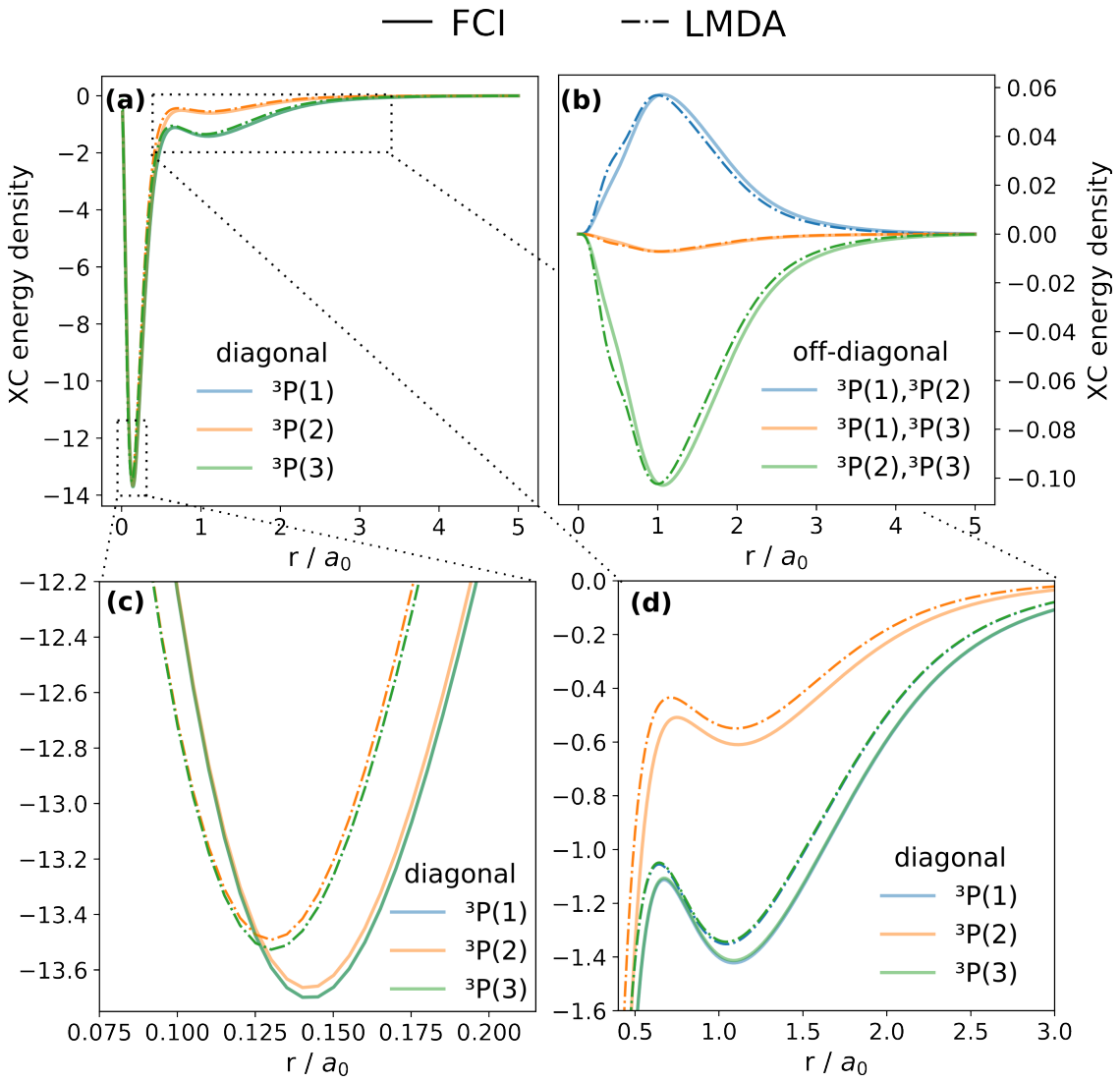

Figure 5: Diagonal (a,c,d) and off-diagonal (b) elements of the exchange-correlation energy density for the lowest ^3P states of the carbon atom, computed exactly (solid line) or with LMDA (Dirac+Chachiyo: dash-dotted line). (c,d) zoom into the regions marked by the dotted rectangle. The curves for all ^3P, ^1D and ^1S states are given in the SI.

Figure 5 compares the exchange-correlation energy densities of the carbon atom along the x-axis obtained from FCI and from MSDFT/LMDA. Using the Dirac exchange and CCA correlation functionals, the LMDA results reproduce the qualitative features of the exact exchange-correlation energy densities over the full spatial range. Both diagonal and off-diagonal matrix elements exhibit the correct overall spatial behavior, including extrema, nodal structure, and asymptotic decay.

For spin multiplets, subspace covariance of the matrix functional is mathematically equivalent to spin-rotational invariance. Both conditions require the exchange-correlation functional to transform covariantly under unitary rotations within the degenerate spin subspace. Consequently, once the multistate matrix density is admitted as the fundamental variable, the long-standing symmetry dilemma of spin-density functional theory is naturally resolved (Fig. 1).

5.3 Atoms

The total energies and vertical excitation energies computed with MSDFT/LMDA for the lowest few electronic states of the atoms H, He, Li, Be, B, C, N, and O are summarized in Tables 1 and 2, together with corresponding FCI and experimental data. The matrix densities were obtained from multistate self-consistent-field (MSSCF) auxiliary wave functions using minimal complete active spaces. Degenerate magnetic sublevels are omitted from the tables for brevity.

The spin-invariant and spin-unpolarized formulations preserve spin symmetry, whereas the spin-polarized representation explicitly breaks spin-rotational invariance through its separate dependence on spin-up and spin-down matrix densities. Only $S_z = 0$ configurations contribute to the active space in the spin-polarized and spin-unpolarized calculations.

Table 1 shows that the LMDA matrix functional generally overestimates total energies relative to FCI, with hydrogen as the notable exception because of self-interaction error. Nevertheless, clear systematic trends emerge among the different spin representations. The spin-invariant functional, $\epsilon_x^{\mathrm{inv}}$, yields the smallest mean absolute error (MAE) relative to FCI, whereas the spin-unpolarized representation, $\epsilon_x^{\mathrm{unpol}}$, exhibits the largest deviations. The mixed representation $\epsilon_x^{\mathrm{mix}}$ gives results comparable to those obtained with the spin-polarized formulation.

Turning to the vertical excitation energies listed in Table 2, we found that the spin-polarized functional, $\epsilon_x^{\mathrm{pol}}$, has the smallest MAE relative to experiment. This improvement

Table 1: Total energies (Hartree) of atomic states determined by full configuration interaction (FCI) and multistate density functional theory with the local multistate-density-approximation (MSDFT/LMDA) using the spin invariant $\epsilon_x^{\mathbf{inv}}$, spin-polarized $\epsilon_x^{\mathbf{pol}}$, spin-unpolarized $\epsilon_x^{\mathbf{unpol}}$, and the equal-weight admixture $\epsilon_x^{\mathbf{mix}}$ functionals. The matrix densities are determined by complete-active-space-self-consistent-field (CAS-SCF) auxiliary states with the number of electrons and orbitals listed under CAS. The electronic configurations (Conf.) and atomic term symbols for different electronic states (Term) are also indicated.

				Total Energy (Hartree)				
Atom	CAS	Conf.	Term	$\epsilon_x^{\mathrm{inv}}$	$\epsilon_x^{\mathrm{pol}}$	$\epsilon_x^{\mathrm{unpol}}$	$\epsilon_x^{\mathrm{mix}}$	FCI
H	(1,5)	1s	^2S	-0.5716	-0.4828	-0.4151	-0.4917	-0.4993
		2p	^2P	-0.1439	-0.0853	-0.0388	-0.0913	-0.0479
		2s	^2S	-0.1737	-0.1436	-0.1207	-0.1467	-0.1219
He	(2,2)	$1s^2$	^1S	-2.8246	-2.7950	-2.7814	-2.7973	-2.8895
		1s2s	^3S	-2.3032	-2.1303	-1.9964	-2.1479	-2.1511
			^1S	-2.1642	-2.0575	-1.9633	-2.0693	-2.0956
Li	(1,4)	$1s^22s$	^2S	-7.3737	-7.3357	-7.3085	-7.3396	-7.4326
		$1s^22p$	^2P	-7.3290	-7.2926	-7.2665	-7.2963	-7.3649
Be	(2,4)	$1s^22s^2$	^1S	-14.5519	-14.4381	-14.3553	-14.4500	-14.6174
		$1s^22s2p$	^3P	-14.4816	-14.3670	-14.2816	-14.3791	-14.5163
			^1P	-14.2810	-14.2317	-14.1936	-14.2370	-14.4107
B	(3,4)	$2s^22p$	^2P	-24.5075	-24.3330	-24.2056	-24.3516	-24.5906
		$2s2p^2$	^4P	-24.4913	-24.2662	-24.0968	-24.2906	-24.4616
C	(2,3)	$2p^2$	^3P	-37.5923	-37.4666	-37.3874	-37.4878	-37.7619
			^1D	-37.4826	-37.4100	-37.3633	-37.4224	-37.7073
			^1S	-37.3181	-37.3251	-37.3271	-37.3243	-37.6542
N	(3,3)	$2p^3$	^4S	-54.3586	-54.1324	-53.9881	-54.1709	-54.4801
			^2D	-54.1633	-54.0297	-53.9438	-54.0525	-54.3802
			^2P	-54.0331	-53.9612	-53.9143	-53.9737	-54.3364
O	(4,3)	$2p^4$	^3P	-74.6713	-74.4991	-74.3880	-74.5287	-74.9117
			^1D	-74.5221	-74.4200	-74.3537	-74.4376	-74.8330
			^1S	-74.2983	-74.3014	-74.3024	-74.3010	-74.7538
		MAE		0.1510	0.2105	0.2739	0.1985	0.0000

arises because symmetry breaking partially compensates for the over-stabilization introduced by coherent spin couplings in the fully invariant formulation. In the spin-rotation-invariant representation $\epsilon_x^{\mathrm{inv}}$, these couplings lower the total energies but increase the excitation gaps.

Table 2: Vertical excitation energies (eV) computed using MSDFT/LMDA and FCI along with the experimental results. See caption of Table 1 for additional details.

				Relative Energy (eV)					
Atom	CAS	Conf.	Term	ϵ_x^{inv}	ϵ_x^{pol}	$\epsilon_x^{\text{unpol}}$	ϵ_x^{mix}	FCI	Expt
H	(1,5)	2p	^2P	11.64	10.82	10.24	10.90	12.29	10.20
		2s	^2S	10.83	9.23	8.01	9.39	10.27	10.20
He	(2,2)	1s2s	^3S	14.19	18.09	21.36	17.67	20.09	19.82
			^1S	17.97	20.07	22.26	19.81	21.60	20.62
Li	(1,4)	$1s^2 2p$	^2P	1.22	1.17	1.14	1.18	1.84	1.85
Be	(2,4)	$1s^2 2s2p$	^3P	1.91	1.94	2.01	1.93	2.75	2.73
			^1P	7.37	5.62	4.40	5.80	5.63	5.28
B	(3,4)	$2s2p^2$	^4P	0.44	1.82	2.96	1.66	3.51	3.55
C	(2,3)	$2p^2$	^1D	2.9'8	1.54	0.66	1.78	1.49	1.26
			^1S	7.46	3.85	1.64	4.45	2.93	2.68
N	(3,3)	$2p^3$	^2D	5.31	2.79	1.21	3.22	2.72	2.38
			^2P	8.86	4.66	2.01	5.37	3.91	3.58
O	(4,3)	$2p^4$	^1D	4.06	2.15	0.93	2.48	2.14	1.97
			^1S	10.15	5.38	2.33	6.20	4.30	4.19
Mean absolute error (MAE)				1.81	0.53	0.71	0.72	0.24	0.00

The spin-unpolarized representation systematically underestimates the excitation energies for the ^1D and ^1S states of C and O and for the ^2D and ^2P states of N, whereas the spin-polarized treatment tends to overestimate them. The mixed representation yields excitation energies for atoms H through O in reasonable agreement with experiment, with an MAE of approximately 0.7 eV.

Given that the present MSDFT/LMDA calculations employ unmodified KS-LDA exchange-correlation functionals the overall performance is highly encouraging. In particular, the ordering of the low-lying electronic states is reproduced correctly for every atom considered here.

Overall, the results reveal a systematic tradeoff between exact spin covariance and excitation energetics. Enforcing full spin covariance improves the description of total energies

through coherent spin mixing, whereas controlled symmetry breaking yields more accurate excitation gaps. The mixed representation provides a balanced overall performance for both total and excitation energies without breaking the spin symmetry.

5.4 H_2 Dissociation and Effect of Spin Structure

Figure 6 compares the potential-energy curves of the four lowest electronic states of H_2, obtained with MSDFT/LMDA/cc-pVDZ using different spin representations of the matrix density functional, together with the corresponding FCI reference curves. The failure of conventional KS-DFT to dissociate H_2 is illustrated by the dashed curves in panel (a): The dissociation energy of S_0 is too large and the S_0 and T_1 are not degenerate in the dissociation limit.

The FCI curves exhibit the correct dissociation limit in which the singlet ground state and triplet state become degenerate as the H−H bond is stretched and the exchange interaction vanishes. This behavior provides a stringent test for approximate multistate matrix functionals because both static correlation and asymptotic spin degeneracy must be described simultaneously.

Panel (a) shows that the spin-invariant representation of the matrix density preserves exact triplet degeneracy throughout the dissociation process, consistent with spin covariance of the matrix functional. However, the triplet state becomes substantially over-stabilized relative to FCI. This behavior reflects residual coherent spin coupling within the degenerate spin manifold that persists even at large H−H separation. At the spectral level, these couplings arise from reordering of the local eigendensity channels within the degenerate spin subspace, causing geometric spin couplings to contribute as effective exchange interactions.

In contrast, the spin-polarized exchange functional in panel (b) yields dissociation curves in much closer agreement with FCI, particularly for the asymptotic singlet-triplet degeneracy. This improvement is achieved by suppressing coherent spin mixing through explicit breaking of spin-rotational invariance. Although the resulting triplet degeneracy is no longer exact,

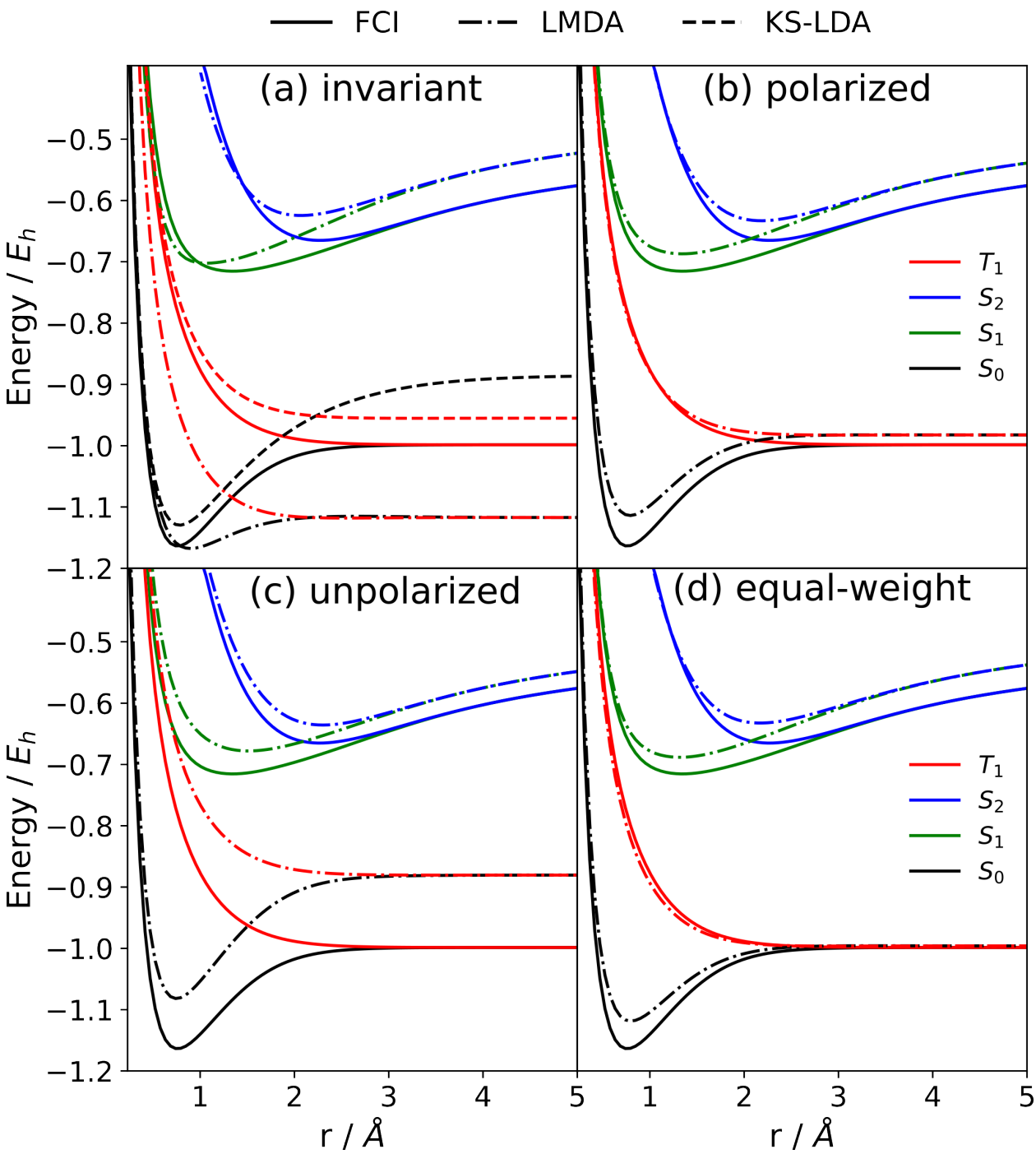

Figure 6: Potential energy curves of H_2 with MSDFT(2e,2o)-LDA/cc-pVDZ vs. FCI and KS-LDA.

the asymptotic energetics are described more accurately because nonphysical residual spin coherence is removed.

Panel (c) shows that the spin-unpolarized representation does not adequately distinguish

singlet and triplet exchange channels because the exchange functional depends only on the spin-traced matrix density. The resulting exchange interaction becomes overly averaged, leading to elevated excitation energies and less accurate dissociation behavior. This behavior is consistent with the local spectral analysis in Fig. 4, where the spin-unpolarized representation cannot properly resolve the exchange splitting between different spin states.

The mixed equal-weight treatment in panel (d) provides the best overall balance. It preserves spin symmetry while avoiding the severe over-stabilization present in the fully invariant representation and substantially improves the asymptotic energetics relative to the spin-unpolarized treatment.

The H_2 dissociation curves in Fig. 6 demonstrate that static correlation and the correct asymptotic singlet-triplet degeneracy emerge naturally within the covariant matrix-functional formalism. As the bond is stretched, the multistate matrix density evolves smoothly from a single-reference regime to the strongly correlated dissociation limit while preserving the proper state structure.

Although different spin matrix-density representations lead to quantitative differences in the dissociation curves, all invariant matrix functionals are generated through a spectral reconstruction procedure using the same local exchange functional. Importantly, essential multistate and static-correlation physics emerge not from new scalar exchange-correlation approximations, but from the covariant multistate matrix-functional structure.

5.5 Ethylene torsion

Figure 7 presents the torsional potential-energy curves of ethylene about the C=C double bond, comparing MSDFT/LMDA with XMS-CASPT2 reference results. As the torsion angle approaches 90°, the π overlap between the two carbon atoms vanishes, producing strong static correlation, substantial multistate mixing, and near degeneracy between the π and π^* orbitals. The twisted geometry therefore approaches a biradical limit in which conventional single-reference KS-DFT and adiabatic TDDFT are known to fail because of

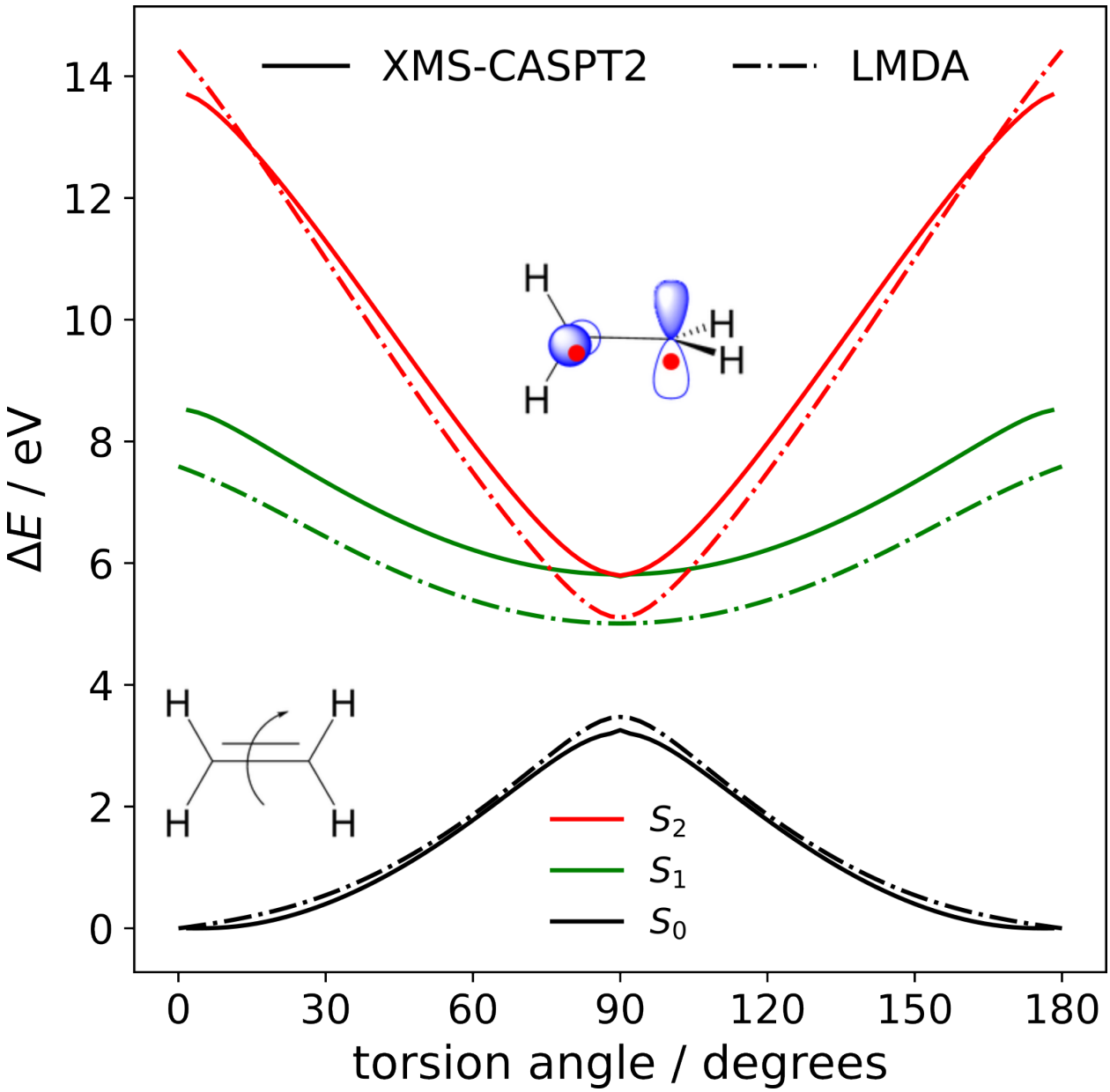

Figure 7: Ethylene torsion scan, MSDFT(2e,2o)/LMDA/cc-pVDZ (dash-dotted) and XMS-CASPT(2e,2o)/cc-pVDZ (solid).

pronounced multireference and double-excitation character.

The ground state (S_0) exhibits a torsional barrier of approximately 3.3 and 3.5 eV from XMS-CASPT2 and MSDFT/LMDA, respectively, corresponding to breaking of the π bond. The excited singlet states (S_1 and S_2) decrease in energy as the torsion angle approaches 90°, reflecting the increasing degeneracy of the bonding and antibonding orbitals. The

MSDFT/LMDA curves reproduce both the topology and energetic ordering of the XMS-CASPT2 curves throughout the torsional rotation. Near the perpendicular geometry, however, the S_1 and S_2 states become somewhat over-stabilized relative to XMS-CASPT2. This excessive energy lowering can be attributed primarily to the self-interaction error of the underlying LDA scalar functional in the strongly correlated near-degenerate regime.[69]

At the equilibrium geometry, the calculated vertical excitation energy of the $^1B_{1u}(\pi \rightarrow \pi^*)$ state is 7.6 eV, in excellent agreement with experiment.[71]

Despite employing the same scalar exchange-correlation functional used in KS-DFT, the present matrix-functional formalism captures the correct qualitative and quantitative multistate behavior throughout the strongly correlated torsional region. As the molecule evolves smoothly from a closed-shell π bond to the twisted biradical limit, the covariant matrix functional preserves the proper state topology and multistate coupling structure.

5.6 Cyclobutadiene Automerization

The automerization of cyclobutadiene is a prototypical test for strong static correlation and multistate electronic structure.[68,72,73] The molecule adopts two equivalent rectangular minima, connected through a square transition-state geometry. As the rectangular structure evolves toward the square geometry, the frontier π orbitals become symmetry-degenerate and the electronic structure acquires pronounced multiconfigurational character. Conventional single-reference approaches therefore encounter substantial difficulty describing both the barrier height and the relative singlet–triplet energetics.

Figure 8 compares the potential-energy curves of the singlet ground state and lowest triplet obtained with MSDFT/LMDA using different spin matrix-density representations of the matrix functional in panels (a-d) and with conventional KS-LDA included in panel (a). The MR-AQCC/SA-4-CASSCF/cc-pVTZ results of Eckert and Maksić serve as the multireference reference curves.[68]

The KS-DFT/LDA results in Fig. 8(a) exhibit several well-known failures associated with

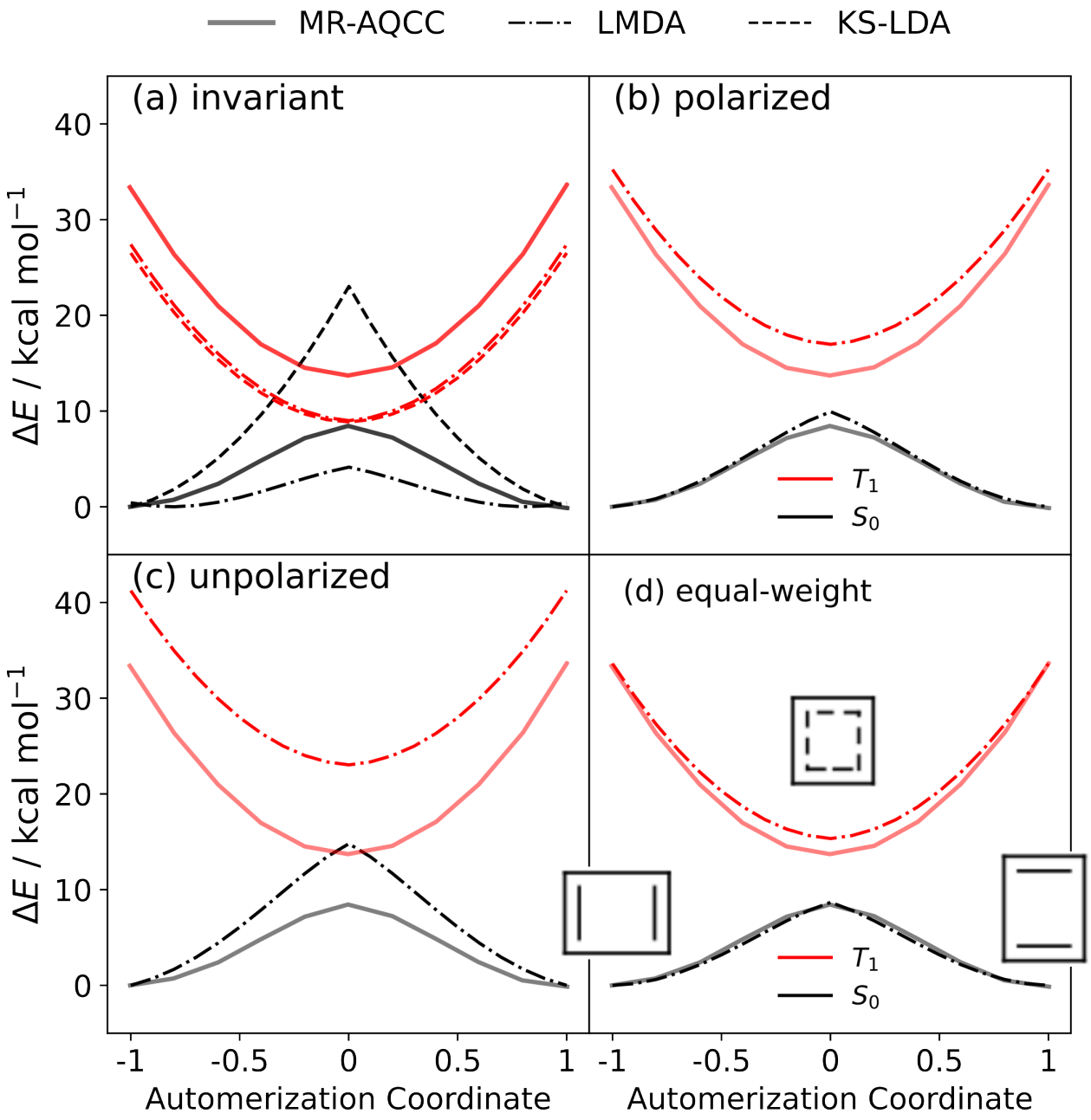

Figure 8: Potential-energy curves for cyclobutadiene automerization computed with MSDFT(4e,4o)/LMDA/cc-pVDZ using different spin representations of the matrix density functional [panels (a–d)]. Solid curves denote the MR-AQCC reference results from Ref.;[68] dash-dotted curves correspond to MSDFT/LMDA and dashed curves to KS-LDA.

strong static correlation. The singlet barrier is substantially overestimated and the singlet surface develops an unphysical cusp near the square geometry. In addition, the singlet-triplet gap becomes negative near the transition state, producing an incorrect energetic ordering of the two spin states. These failures originate from the inability of a single Slater determinant

to smoothly describe the transition from a bond-localized electronic structure to the strongly multiconfigurational regime associated with the square geometry.

In contrast, the multistate matrix-functional treatment captures the essential static-correlation physics by explicitly including the interaction among the near-degenerate π-electron configurations within the active space. As shown in Fig. 8(a-d), all spin representations of the MSDFT/LMDA functional yield qualitatively correct potential-energy curves with positive singlet-triplet gaps throughout the automerization pathway. Among these, the equal-weight mixed representation provides the best overall agreement with the MR-AQCC reference curves.

The barrier height obtained with the mixed representation is 8.7 kcal mol^{-1}, in excellent agreement with the best theoretical estimate of 8.8 kcal mol^{-1} from extrapolated MR-AQCC/TQ calculations.[74] The calculated singlet–triplet splitting is likewise accurate, giving 6.6 kcal mol^{-1} compared with the MR-AQCC value of 5.3 kcal mol^{-1}. Higher excited-state curves (not shown) exhibit the correct qualitative topology but are shifted upward in energy because the ROHF orbitals were not variationally optimized in this case.

6 Conclusion

A local matrix density approximation (LMDA) within multistate density functional theory has been developed and demonstrated, for the first time, through fully variational calculations of excited states of atoms and small molecules. The formulation is based on covariance of the Hamiltonian matrix functional and reduces to KS-DFT in the single-state limit. Covariance under similarity transformations dictates that the matrix functional for LDA exchange and correlation is uniquely defined by the corresponding scalar functional via a spectral decomposition of the matrix density.

Applications to atomic excitations, H_2 dissociation, ethylene torsion and cyclobutadiene automerization show that the matrix-version of LDA captures essential multistate and

strong-correlation physics, including static correlation and spin-multiplet degeneracy. This unexpected accuracy in situations where conventional KS-LDA fails can be explained by the normalization of the exchange-correlation hole *matrix*, which is fulfilled exactly by LMDA. The degeneracy of spin multiplets also emerges naturally thanks to the covariance property of matrix functionals, since a rotation of the spin vector corresponds to a similarity transformation of the spin matrix density.

The present results suggest that the extension of density functional theory to interacting electronic states does not necessarily require more complex scalar exchange-correlation approximations, but rather a covariant matrix-functional formalism in which such functionals can operate.

AUTHOR INFORMATION

Corresponding Authors

Alexander Humeniuk - Independent Researcher, orcid.org/0000-0002-3748-4921; Email: alexander.humeniuk@gmail.com

Yangyi Lu - Institute of Systems and Physical Biology, Shenzhen Bay Laboratory, Shenzhen 518107, China; orcid.org/0000-0002-1602-1661; Email: luyy@szbl.ac.cn

Authors

Jiali Gao - Institute of Systems and Physical Biology, Shenzhen Bay Laboratory, Shenzhen 518107, China; School of Chemical Biology and Biotechnology, Shenzhen Graduate School Peking University, Shenzhen 518055, China; Department of Chemistry and Supercomputing Institute, University of Minnesota, Minneapolis, Minnesota 55455, United States; orcid.org/0000-0003-0106-7154; Email: gao@jialigao.org

Notes

The authors declare no competing financial interest.

Acknowledgement

A.H. thanks Michael Römelt and HPC@HU of Humboldt University Berlin for computational resources. This work has been partially supported by the National Natural Science Foundation of China (Grants No.22522307 and No.12304285), the Guangdong Basic and Applied Basic Research Foundation (No.2023A1515011237), and the PI start-up fund and the high-performance computing facility at Shenzhen Bay Laboratory. Work carried out at Minnesota was supported by the National Institutes of Health (Grant GM046736).

Appendix

A Normalization of exchange-correlation hole matrix

The normalization of the XC hole is derived as follows.

Integrating the pair density using eq 11 over the second coordinate gives

$$\int d^3r' D_{IJ}^{(2e)}(\mathbf{r}, \mathbf{r}') = (n-1) D_{IJ}(\mathbf{r}) \tag{A1}$$

Similarly, integrating the result of eq 12 yields

$$\sum_K D_{IK}(\mathbf{r}) \int d^3r' \left[D_{KJ}(\mathbf{r}') + H_{KJ}^{\mathrm{xc}}(\mathbf{r}, \mathbf{r}') \right] = \sum_K D_{IK}(\mathbf{r}) \left[n\delta_{KJ} + \int d^3r' H_{KJ}^{\mathrm{xc}}(\mathbf{r}, \mathbf{r}') \right] \tag{A2}$$

Since the left-hand side of both equations are the same, we have

$$(n-1) D_{IJ}(\mathbf{r}) = n D_{IJ}(\mathbf{r}) + \sum_K D_{IK}(\mathbf{r}) \int d^3r' H_{KJ}^{\mathrm{xc}}(\mathbf{r}, \mathbf{r}') \tag{A3}$$

Multiplying both sides with the inverse of the matrix density shows that the exchange-correlation hole has to integrate to (-1) times the identity matrix for any reference point $\mathbf{r}$:

$$\int H_{IJ}^{\mathrm{xc}}(\mathbf{r}, \mathbf{r}') d^3r' = -\delta_{IJ} \quad \forall \mathbf{r} \tag{A4}$$

B Taylor expansion of spherically-averaged exchange matrix hole

Becke showed that the Taylor expansion of the exchange hole $\rho_{x\uparrow}$ in the coordinate $\mathbf{u}$ about the reference point $\mathbf{r}$ is[53]

$$\rho_{x\uparrow}(\mathbf{r},u) = -\langle e^{\mathbf{u}\cdot\nabla_1}\rangle \rho_{x\uparrow}(\mathbf{r},\mathbf{r}_1)\Big|_{\mathbf{r}_1=\mathbf{r}} \tag{B1}$$

$$= -\rho_\uparrow(\mathbf{r}) - \frac{1}{6}\left(\nabla^2\rho_\uparrow(\mathbf{r}) + 4\Delta t(\mathbf{r})\right)u^2 + \ldots \tag{B2}$$

where $\Delta t(\mathbf{r}) = t_{vW}(\mathbf{r}) - t(\mathbf{r})$ is the difference between the von Weizsäcker (vW) kinetic energy density $t_{vW} = \frac{1}{8}(|\nabla\rho_\uparrow|^2/\rho_\uparrow)$ and the Kohn-Sham kinetic energy density computed from the orbitals, $t = \frac{1}{2}\sum_i |\nabla\phi_i(\mathbf{r})|^2$. For a single electron with real wavefunction $\phi(\mathbf{r})$, where the density is $\rho_\uparrow(\mathbf{r}) = \phi(\mathbf{r})^2$, the von Weizsäcker kinetic energy density becomes exact, so that Δt vanishes. Deriving an analogous expression for the matrix exchange hole is considerably more difficult because, unlike Kohn–Sham theory, there is no corresponding reference system of noninteracting electrons that provides single-particle orbitals and an associated kinetic-energy functional.

We start with the matrix density for a one-electron system, which is just the product of the orbitals,

$$D_{IJ}(\mathbf{r}) = \phi_I(\mathbf{r})\phi_J(\mathbf{r}). \tag{B3}$$

Since there is no interaction with other electrons, the exact exchange hole is independent of the reference point, $H^x_{IJ}(\mathbf{r},\mathbf{r}') = -D_{IJ}(\mathbf{r}')$. Therefore, the exchange energy exactly cancels the Hartree term.

Now, we consider the expression of the exchange matrix hole

$$H^x_{IJ}(\mathbf{r},\mathbf{r}_1) = -\sum_K \left(\mathbf{D}^{-1}(\mathbf{r})\right)_{IK}\left(\sum_L D_{KL}(\mathbf{r},\mathbf{r}_1)D_{LJ}(\mathbf{r},\mathbf{r}_1)\right) \tag{B4}$$

and perform a spherically-averaged Taylor expansion in $\mathbf{r}_1$ around the reference point $\mathbf{r}$ with D_{IJ} taken from eq B3. The resulting Taylor expansion for the one-electron system, expressed in terms of the matrix density and its derivatives, is then assumed to be valid for any matrix density. Since for a matrix density of a single electron

$$\left[\nabla_1^2 \sum_L D_{KL}(\mathbf{r},\mathbf{r}_1) D_{LJ}(\mathbf{r},\mathbf{r}_1)\right]_{\mathbf{r}_1=\mathbf{r}} = \left[\nabla_1^2 \sum_L \phi_K(\mathbf{r})\phi_L(\mathbf{r}_1)\phi_L(\mathbf{r})\phi_J(\mathbf{r}_1)\right] \tag{B5}$$

$$= \sum_L D_{KL}\left(\phi_J \nabla^2\phi_L + (\nabla^2\phi_J)\phi_L + 2\nabla\phi_J\cdot\nabla\phi_L\right), \tag{B6}$$

one finds that

$$\nabla_1^2 H^x_{IJ}(\mathbf{r},\mathbf{r}_1)\Big|_{\mathbf{r}_1=\mathbf{r}} = -\sum_L \underbrace{\sum_K \left(\mathbf{D}^{-1}(\mathbf{r})\right)_{IK} D_{KL}(\mathbf{r})}_{\delta_{IL}} \underbrace{\left(\phi_J\nabla^2\phi_L + (\nabla^2\phi_J)\phi_L + 2\nabla\phi_J\cdot\phi_L\right)}_{\nabla^2 D_{LJ}(\mathbf{r})}, \tag{B7}$$

so that for small distances u from the reference point the spherically averaged exchange matrix hole to second order becomes

$$\langle H^x_{IJ}\rangle(\mathbf{r},u) = -D_{IJ}(\mathbf{r}) - \frac{1}{6}\nabla^2 D_{IJ}(\mathbf{r})u^2 - \ldots \tag{B8}$$

Since this is derived for a one-electron matrix density it lacks the kinetic term Δt of equation B2. Nevertheless, this is a reasonable approximation for the exchange hole close to the reference point, which is shown by comparison with exact exchange-correlation holes computed from ab initio wavefunctions in Fig. 3.

C Simple examples for spin matrix densities

C.1 One electron: doublet ground state of hydrogen atom

The hydrogen atom has only electron ($n = 1$) which can be in either of the two spin states. The spinor wavefunctions for spin up and spin down are denoted by $\alpha(\mathbf{s}) = (1, 0)^T$ and $\beta(\mathbf{s}) = (0, 1)^T$. The doublet ground state is two-fold degenerate forming a subspace of $N = 2$ states,

$$\psi_1(\mathbf{r}, \mathbf{s}) = \phi_{1s}(\mathbf{r})\alpha(\mathbf{s}) = \phi_{1s}(\mathbf{r}) \begin{pmatrix} 1 \\ 0 \end{pmatrix} \tag{C1}$$

$$\psi_2(\mathbf{r}, \mathbf{s}) = \phi_{1s}(\mathbf{r})\beta(\mathbf{s}) = \phi_{1s}(\mathbf{r}) \begin{pmatrix} 0 \\ 1 \end{pmatrix} \tag{C2}$$

Both states have the same spatial wavefunction $\phi_{1s}(\mathbf{r})$ and the same charge density $\rho = |\phi_{1s}(\mathbf{r})|^2$. According to eq 23 the spin matrix density is the 4×4 matrix below,

$$\tilde{\mathbf{D}}(\mathbf{r}) = n \begin{pmatrix} \psi_1\psi_1^\dagger & \psi_1\psi_2^\dagger \\ \psi_2\psi_1^\dagger & \psi_2\psi_2^\dagger \end{pmatrix} = n|\psi_{1s}(\mathbf{r})|^2 \begin{pmatrix} \alpha\alpha^\dagger & \alpha\beta^\dagger \\ \beta\alpha^\dagger & \beta\beta^\dagger \end{pmatrix}. \tag{C3}$$

Explicitly, by writing out the outer products of the spinors, we have

$$\tilde{\mathbf{D}}(\mathbf{r}) = \rho(\mathbf{r}) \begin{array}{c} \\ \\ \alpha \\ \beta \\ \alpha \\ \beta \end{array} \begin{array}{c} \begin{array}{cccc} J=1 & & J=2 & \\ \alpha & \beta & \alpha & \beta \end{array} \\ \begin{pmatrix} 1 & 0 & 0 & 1 \\ 0 & 0 & 0 & 0 \\ 0 & 0 & 0 & 0 \\ 1 & 0 & 0 & 1 \end{pmatrix} \end{array} \begin{array}{l} \\ \\ I=1 \\ \\ I=2 \\ \\ \end{array}. \tag{C4}$$

The spin matrix density has only one eigenvalue different from zero, as there are two zero columns and columns one and four are linearly dependent. $\tilde{\mathbf{D}}$ has the eigendecomposition $\tilde{\mathbf{D}} = \mathbf{U}\,\mathrm{diag}(\mathbf{d})\mathbf{U}^{-1}$ in terms of the eigenvalues

$$\mathbf{d} = (0, 0, 0, 2\rho(\mathbf{r})) \tag{C5}$$

and eigenvectors

$$\mathbf{U} = \begin{pmatrix} 0 & 1 & 0 & 0 \\ 0 & 0 & 1 & 0 \\ -1 & 0 & 0 & 1 \\ 1 & 0 & 0 & 1 \end{pmatrix} \tag{C6}$$

Let us assume for simplicity that the functional for the energy density is local, i.e. $f(\rho)$. Then the energy density matrix is

$$\mathbf{F}[\tilde{\mathbf{D}}] = \mathbf{U}\,\mathrm{diag}(0, 0, 0, f(2\rho(\mathbf{r})))\mathbf{U}^{-1} = \begin{pmatrix} \frac{f(2\rho)}{2} & 0 & 0 & \frac{f(2\rho)}{2} \\ 0 & 0 & 0 & \\ 0 & 0 & 0 & \\ \frac{f(2\rho)}{2} & 0 & 0 & \frac{f(2\rho)}{2} \end{pmatrix} \tag{C7}$$

Taking the spin trace and integrating over space the Hamiltonian matrix for the two doublet states becomes

$$\mathbf{H} = \int d^3r \;\; \mathrm{spintrace}(\mathbf{F}(\mathbf{r})) = \begin{pmatrix} \int \frac{f(2\rho(\mathbf{r}))}{2} & 0 \\ 0 & \int \frac{f(2\rho(\mathbf{r}))}{2} \end{pmatrix} \tag{C8}$$

As expected there is no coupling between the doublet states and they have the same energy.

Having illustrated this trivial example, we move to a more complicated case with electronic couplings.

C.2 Two electrons: singlet-triplet splitting

The system consists of $n = 2$ electrons in two orthonormal orbitals (e.g. HOMO $\phi_H(\mathbf{r})$ and LUMO $\phi_L(\mathbf{r})$) and we focus on the subspace where the electrons are in different spatial orbitals. This subspace consists of the open-shell singlet and the three components of the triplet. The closed-shell singlet ground state is left out for simplicity. The wavefunctions are products of the spatial wavefunctions

$$\Phi_{\text{singlet}}(1,2) = \frac{1}{\sqrt{2}}\left(\phi_H(1)\phi_L(2) + \phi_L(1)\phi_H(2)\right) \tag{C9}$$

$$\Phi_{\text{triplet}}(1,2) = \frac{1}{\sqrt{2}}\left(\phi_H(1)\phi_L(2) - \phi_L(1)\phi_H(2)\right) \tag{C10}$$

and the spin wavefunctions

$$\chi(S=0, S_z=0) = \frac{1}{\sqrt{2}}\left(\alpha(1)\beta(2) - \beta(1)\alpha(2)\right) \tag{C11}$$

$$\chi(S=1, S_z=-1) = \beta(1)\beta(2) \tag{C12}$$

$$\chi(S=1, S_z=0) = \frac{1}{\sqrt{2}}\left(\alpha(1)\beta(2) + \beta(1)\alpha(2)\right) \tag{C13}$$

$$\chi(S=1, S_z=+1) = \alpha(1)\alpha(2) \tag{C14}$$

The arguments 1 and 2 denote the spatial and/or spin degrees of freedom depending on the context. The wavefunction for the open-shell singlet is

$$\Psi_{S,0} = \Phi_{\text{singlet}}(1,2)\chi(S=0, S_z=0) \tag{C15}$$

and the three components of the triplet state are

$$\Psi_{T,-1} = \Psi_{\text{triplet}}(1,2)\chi(S=1,S_z=-1) \tag{C16}$$

$$\Psi_{T,0} = \Psi_{\text{triplet}}(1,2)\chi(S=1,S_z=0) \tag{C17}$$

$$\Psi_{T,+1} = \Psi_{\text{triplet}}(1,2)\chi(S=1,S_z=+1) \tag{C18}$$

The spin matrix density is calculated by integrating out the second electron's spatial and spin coordinates in

$$\tilde{D}_{IJ}^{\sigma\sigma'}(\mathbf{r},\mathbf{r}') = n\int \Psi_I(1,2)\Psi_J^*(1',2)d2 \tag{C19}$$

and setting $\mathbf{r}' = \mathbf{r}$ in the end,

$$\tilde{D}_{IJ}^{\sigma\sigma'}(\mathbf{r}) = D_{IJ}^{\sigma\sigma'}(\mathbf{r},\mathbf{r}'=\mathbf{r}) \tag{C20}$$

The unique integrals over the spatial coordinate of the second electron are

$$\int \Phi_{\text{singlet}}(1,2)\Phi_{\text{singlet}}(1',2)^* d2 = \int \Phi_{\text{triplet}}(1,2)\Phi_{\text{triplet}}(1',2)^* d2 \tag{C21}$$

$$= \frac{1}{2}\left(\phi_H(1)\phi_H^*(1') + \phi_L(1)\phi_L^*(1')\right) \tag{C22}$$

$$\int \Phi_{\text{singlet}}(1,2)\Phi_{\text{triplet}}(1',2)^* d2 = \frac{1}{2}\left(\phi_H(1)\phi_H^*(1') - \phi_L(1)\phi_L^*(1')\right) \tag{C23}$$

With the abbreviations

$$\rho(\mathbf{r}) = \frac{n}{2}\left(|\phi_H(\mathbf{r})|^2 + |\phi_L(\mathbf{r})|^2\right), \tag{C24}$$

$$\Delta(\mathbf{r}) = \frac{n}{2}\left(|\phi_H(\mathbf{r})|^2 - |\phi_L(\mathbf{r})|^2\right) \tag{C25}$$

and

$$\xi = \frac{\Delta}{\rho} \tag{C26}$$

the spatial part of the matrix density becomes

$$\rho \begin{array}{c} \begin{array}{cc} \text{singlet} & \text{triplet} \end{array} \\ \begin{pmatrix} 1 & \xi \\ \xi & 1 \end{pmatrix} \begin{array}{c} \text{singlet} \\ \text{triplet} \end{array} \end{array} . \tag{C27}$$

The integrals over the spin degrees of freedom of the second electron consist of

- the singlet block

$$\begin{aligned} &\int \chi(S=0,S_z=0)\chi(S=0,S_z=0)^* d2 \\ &= \frac{1}{2}\int d2\left[\alpha(1)\beta(2)-\beta(1)\alpha(2)\right]\left[\alpha^*(1')\beta^*(2)-\beta^*(1')\alpha^*(2)\right] \\ &= \frac{1}{2}\left(\alpha(1)\alpha^*(1')+\beta(1)\beta^*(1')\right) \end{aligned} \tag{C28}$$

- the singlet-triplet blocks

$$\int \chi(S=0,S_z=0)\chi(S=1,S_z=-1)^* d2 = \frac{1}{\sqrt{2}}\alpha(1)\beta^*(1') \tag{C29}$$

$$\int \chi(S=0,S_z=0)\chi(S=1,S_z=0)^* d2 = \frac{1}{2}\left(\alpha(1)\alpha^*(1')-\beta(1)\beta^*(1')\right) \tag{C30}$$

$$\int \chi(S=0,S_z=0)\chi(S=1,S_z=+1)^* d2 = -\frac{1}{\sqrt{2}}\beta(1)\alpha^*(1') \tag{C31}$$

- and the triplet-triplet blocks

$$\int \chi(S=1,S_z=-1)\chi(S=1,S_z=-1)^* d2 = \beta(1)\beta^*(1') \tag{C32}$$

$$\int \chi(S=1,S_z=-1)\chi(S=1,S_z=0)^* d2 = \frac{1}{\sqrt{2}}\beta(1)\alpha^*(1') \tag{C33}$$

$$\int \chi(S=1,S_z=-1)\chi(S=1,S_z=+1)^* d2 = 0 \tag{C34}$$

$$\int \chi(S=1,S_z=0)\chi(S=1,S_z=0)^* d2 = \frac{1}{2}\left(\alpha(1)\alpha^*(1') + \beta(1)\beta^*(1')\right) \tag{C35}$$

$$\int \chi(S=1,S_z=+1)\chi(S=1,S_z=0)^* d2 = \frac{1}{\sqrt{2}}\alpha(1)\beta^*(1') \tag{C36}$$

$$\int \chi(S=1,S_z=+1)\chi(S=1,S_z=+1)^* d2 = \alpha(1)\alpha^*(1') \tag{C37}$$

Combining spatial and spin parts, the spin matrix density becomes

$$\left(\tilde{D}_{IJ}^{\sigma\sigma'}\right) = \rho \begin{array}{c} \begin{array}{cccccccc} S=0 & & & & S=1 & & & \\ S_z=0 & & S_z=-1 & & S_z=0 & & S_z=+1 & \\ \alpha & \beta & \alpha & \beta & \alpha & \beta & \alpha & \beta \end{array} \\ \begin{pmatrix} \frac{1}{2} & 0 & 0 & \frac{\xi}{\sqrt{2}} & \frac{\xi}{2} & 0 & 0 & 0 \\ 0 & \frac{1}{2} & 0 & 0 & 0 & -\frac{\xi}{2} & -\frac{\xi}{\sqrt{2}} & 0 \\ 0 & 0 & 0 & 0 & 0 & 0 & 0 & 0 \\ \frac{\xi}{\sqrt{2}} & 0 & 0 & 1 & \frac{1}{\sqrt{2}} & 0 & 0 & 0 \\ \frac{\xi}{2} & 0 & 0 & \frac{1}{\sqrt{2}} & \frac{1}{2} & 0 & 0 & 0 \\ 0 & -\frac{\xi}{2} & 0 & 0 & 0 & \frac{1}{2} & \frac{1}{\sqrt{2}} & 0 \\ 0 & -\frac{\xi}{\sqrt{2}} & 0 & 0 & 0 & \frac{1}{\sqrt{2}} & 1 & 0 \\ 0 & 0 & 0 & 0 & 0 & 0 & 0 & 0 \end{pmatrix} \end{array} . \tag{C38}$$

Note that it does not matter if one writes the spin matrix density as a $N \times N$ block matrix of 2×2 blocks or a 2×2 matrix of the the four $N \times N$ blocks $\mathbf{D}^{\alpha\alpha}, \mathbf{D}^{\alpha\beta}, \mathbf{D}^{\beta\alpha}, \mathbf{D}^{\beta\beta}$. We choose one representation or the other depending on which one is more convenient.

The following properties of the spin matrix are immediately apparent:

- Columns 3 and 8 are zero vectors.
- Columns 4 and 5 a linearly dependent: $\mathbf{c}_5 = \frac{1}{\sqrt{2}}\mathbf{c}_4$.
- Columns 6 and 7 are linearly dependent: $\mathbf{c}_6 = \frac{1}{\sqrt{2}}\mathbf{c}_7$.

Therefore the spin matrix must have 4 nonzero singular eigenvalues, which are given below, determined with the sympy library for symbolic computation.[75]

Eigenvalue	Algebratic multiplicity
$d_0 = 0$	4
$d_- = \rho\left(1 - \frac{1}{2}\sqrt{3\xi^2 + 1}\right)$	2
$d_+ = \rho\left(1 + \frac{1}{2}\sqrt{3\xi^2 + 1}\right)$	2

Since $\rho \geq 0$ and $0 \leq \xi^2 \leq 1$, all eigenvalues are ≥ 0, and therefore the spin matrix density is positive definite as expected.

For simplicity, we consider the exchange functional within the local density approximation. The matrix functional associated with Dirac exchange, $\mathbf{F}(\tilde{\mathbf{D}}) = -C_x\tilde{\mathbf{D}}^{4/3}$, is constructed through spectral decomposition: the matrix density is first diagonalized, the scalar exchange function $\epsilon_x(d) = -C_x d^{4/3}$ is evaluated for the eigendensities $d_{0/-/+}$, and the resulting matrix is transformed back to the original representation.

D Chain rule of calculus for matrix functions

A complication with matrix functions (or functionals) is that the usual chain rule of differentiation is not valid anymore.[76] Computing the derivative of a matrix function therefore is somewhat involved. Let's suppose we have a matrix function $\mathbf{X}(t) : \mathbb{R} \to \mathbb{C}^{N\times N}$ which does not commute with its derivative, $[\mathbf{X}(t), d\mathbf{X}/dt] \neq 0$. The Taylor series of the analytical scalar function $f(x) : \mathbb{C} \to \mathbb{C}$ defines an analytical matrix function $\mathbf{F}(\mathbf{X}) : \mathbb{C}^{N\times N} \to \mathbb{C}^{N\times N}$.

To calculate the derivative $d\mathbf{F}[\mathbf{X}(t)]/dt$ of $\mathbf{F}$ with respect to the external parameter t the usual chain rule of calculus is no longer simply applicable: $d\mathbf{F}[\mathbf{X}(t)]/dt \neq \mathbf{F}'(\mathbf{X})(d\mathbf{X}/dt)$.

Instead $\frac{d\mathbf{F}}{dt}$ is calculated as follows: One starts by decomposing $\mathbf{X}(t)$ into its eigenvalues $\mathbf{\Lambda}(t)$ and eigenvectors $\mathbf{U}(t)$,

$$\mathbf{X}(t) = \mathbf{U}(t)\mathbf{\Lambda}(t)\mathbf{U}^{\dagger}(t). \tag{D1}$$

The analytic matrix function $\mathbf{F}(\mathbf{X})$ is defined by the scalar function $f(x)$, which operates on the eigenvalues of $\mathbf{X}$,

$$\mathbf{F}(t) = \mathbf{F}(\mathbf{X}(t)) = \mathbf{U}(t)f(\mathbf{\Lambda}(t))\mathbf{U}^{\dagger}(t). \tag{D2}$$

As shown in the SI, the derivative of the matrix function with respect to the parameters t becomes

$$\frac{d\mathbf{F}}{dt} = \sum_{\alpha=1}^{N}\sum_{\beta=1}^{N}\mathbf{P}_{\alpha}\frac{d\mathbf{X}}{dt}\mathbf{P}_{\beta} \times \begin{cases} f'(\lambda_\alpha) & \text{if} \quad \lambda_\alpha = \lambda_\beta \\ \frac{f(\lambda_\alpha)-f(\lambda_\beta)}{\lambda_\alpha-\lambda_\beta} & \text{if} \quad \lambda_\alpha \neq \lambda_\beta \end{cases}, \tag{D3}$$

where the sums are over the eigenvalues λ_α and the projectors onto the corresponding eigenvectors are $(\mathbf{P}_\alpha)_{ij} = U_{i\alpha}U_{j\alpha}$. In terms of the eigenvectors the derivative of the matrix function becomes

$$\left[\frac{dF}{dt}\right]_{ij} = \sum_{\alpha}\sum_{\beta} U_{i\alpha}\left(\left(\sum_{k}\sum_{l} U_{k\alpha}\left[\frac{dX}{dt}\right]_{kl} U_{l\beta}\right) Y_{\alpha\beta}\right) U_{j\beta} \tag{D4}$$

with

$$Y_{\alpha\beta} = \begin{cases} f'(\lambda_\alpha) & \text{if} \quad \lambda_\alpha = \lambda_\beta \\ \frac{f(\lambda_\alpha)-f(\lambda_\beta)}{\lambda_\alpha-\lambda_\beta} & \text{if} \quad \lambda_\alpha \neq \lambda_\beta. \end{cases} \tag{D5}$$

E Backpropagation of gradients through matrix functions

For backpropagation through a neural network composed of analytic matrix functions using pytorch's *autograd*[60] mechanism, we are interested in the gradient of a scalar function $g = g(\mathbf{F}(\mathbf{X}))$ with respect to $\mathbf{X}$:

$$\frac{\partial g}{\partial X_{kl}} = \sum_i \sum_j \underbrace{\frac{\partial g}{\partial F_{ij}}}_{\mathbf{v}} \cdot \underbrace{\frac{\partial F_{ij}}{\partial X_{kl}}}_{\mathbf{J}^T} \tag{E1}$$

where the vector $\mathbf{v}$ is the gradient of g w.r.t. $\mathbf{F}$, and $\mathbf{J}^T$ represents the transpose of the Jacobian of the mapping $\mathbf{X} \mapsto \mathbf{F}(\mathbf{X})$. Here, in practice, $\mathbf{v}$ is flattened into a long vector (vectorization), which represents the sensitivity of the scalar g to each entry of the matrix $\mathbf{F}$, and the full Jacobian $\mathbf{J}$ is a very large matrix that contains all partial derivatives $\partial F_{ij}/\partial X_{kl}$. The entire expression is compactly written in matrix form as:

$$\nabla_{\mathbf{X}} g = \mathbf{J}^T \mathbf{v}$$

This is the vector-Jacobian product, used as the core operation in reverse-mode automatic differentiation (backpropagation).

In practice, the vector $\mathbf{v}$ is passed as the input to the `backward` function. (Because v_{ij} has two indices it would be more appropriate to call it a matrix, but we interpret it as a vector with N^2 elements to be consistent with pytorch's notation). Comparison with eq D4 shows that the vector-Jacobian product can be evaluated as

$$\frac{\partial g}{\partial X_{kl}} = \sum_{\alpha,\beta} U_{k\alpha} \left[Y_{\alpha\beta} \left(\sum_{i,j} U_{i\alpha} v_{ij} U_{j\beta} \right) \right] U_{l\beta} \tag{E2}$$

The eigenvalues $\mathbf{\Lambda}$ and eigenvectors $\mathbf{U}$ only need to be computed once in the forward pass

and can be reused in the backward pass.

References

(1) Hohenberg, P.; Kohn, W. Inhomogeneous electron gas. *Phys. Rev.* **1964**, *136*, B864–B871.

(2) Kohn, W.; Sham, L. J. Self-consistent equations including exchange and correlation effects. *Phys. Rev.* **1965**, *140*, A1133–A1138.

(3) Parr, R. G.; Yang, W. *Density-Functional Theory of Atoms and Molecules*; Oxford University Press, 1989.

(4) Bechstedt, F. In *Many-Body Approach to Electronic Excitations*, 1st ed.; Cardona, M., von Klitzing, K., Merlin, R., Queisser, H.-J., Eds.; Springer: Berlin, Heidelberg, 2015; Vol. 181; p 584, DOI: 10.1007/978-3-662-44593-8␣ISSN.

(5) Becke, A. D. Perspective: Fifty years of density-functional theory in chemical physics. *J. Chem. Phys.* **2014**, *140*, 1–18, DOI: 10.1063/1.4869598.

(6) Burke, K. Perspective on density functional theory. *J. Chem. Phys.* **2012**, *136*, DOI: 10.1063/1.4704546.

(7) Jones, R. O. Density functional theory: Its origins, rise to prominence, and future. *Rev. Mod. Phys.* **2015**, *87*, 897–923, DOI: 10.1103/RevModPhys.87.897.

(8) Cramer, C. J.; Truhlar, D. G. Density functional theory for transition metals and transition metal chemistry. *Phys. Chem. Chem. Phys.* **2009**, *11*, 10757–10816, DOI: 10.1039/b907148b.

(9) Cheng, G. J.; Zhang, X.; Chung, L. W.; Xu, L.; Wu, Y. D. Computational organic chemistry: Bridging theory and experiment in establishing the mechanisms of chemical reactions. *J. Am. Chem. Soc.* **2015**, *137*, 1706–1725, DOI: 10.1021/ja5112749.

(10) Shang, H.; Xu, L.; Wu, B.; Qin, X.; Zhang, Y.; Yang, J. The dynamic parallel distribution algorithm for hybrid density-functional calculations in HONPAS package. *Computer Physics Communications* **2020**, *254*, 107204, DOI: https://doi.org/10.1016/j.cpc.2020.107204.

(11) Erba, A.; Baima, J.; Bush, I.; Orlando, R.; Dovesi, R. Large-Scale Condensed Matter DFT Simulations: Performance and Capabilities of the CRYSTAL Code. *J. Chem. Theory Comp.* **2017**, *13*, 5019–5027, DOI: 10.1021/acs.jctc.7b00687.

(12) Nakata, A.; Baker, J. S.; Mujahed, S. Y.; Poulton, J. T. L.; Arapan, S.; Lin, J.; Raza, Z.; Yadav, S.; Truflandier, L.; Miyazaki, T. et al. Large scale and linear scaling DFT with the CONQUEST code. *J. Chem. Phys.* **2020**, *152*, 164112, DOI: 10.1063/5.0005074.

(13) Cole, D. J.; Hine, N. D. M. Applications of large-scale density functional theory in biology. *J. Phys. Condensed Matter* **2016**, *28*, 393001, DOI: 10.1088/0953-8984/28/39/393001.

(14) Runge, E.; Gross, E. K. Density-functional theory for time-dependent systems. *Phys. Rev. Lett.* **1984**, *52*, 997–1000.

(15) Casida, M. E. *Recent Advances In Density Functional Methods: (Part I)*; World Scientific, 1995; pp 155–192.

(16) Marques, M. A. L.; Gross, E. K. U. Time-dependent density functional theory. *Annu. Rev. Phys. Chem.* **2004**, *55*, 427–455, DOI: 10.1146/annurev.physchem.55.091602.094449.

(17) Marques, M. A. L.; Ullrich, C. A.; Nogueira, F.; Rubio, A.; Burke, K.; Gross, E. K. U. *Time-dependent density Functional theory*; The Lecture Notes in Physics; Springer, 2006; p 603, DOI: /10.1007/b11767107.

(18) Dreuw, A.; Head-Gordon, M. Failure of Time-Dependent Density Functional Theory for Long-Range Charge-Transfer Excited States: The Zincbacteriochlorin Bacteriochlorin and Bacteriochlorophyll Spheroidene Complexes. *J. Am. Chem. Soc.* **2004**, *126*, 4007–4016, DOI: 10.1021/ja039556n.

(19) Levine, B. G.; Ko, C.; Quenneville, J.; Martínez, T. J. Conical intersections and double excitations in time-dependent density functional theory. *Mol. Phys.* **2006**, *104*, 1039–1051.

(20) Maitra, N. T. Perspective: Fundamental aspects of time-dependent density functional theory. *J. Chem. Phys.* **2016**, *144*, DOI: 10.1063/1.4953039.

(21) Maitra, N. T. Double and Charge-Transfer Excitations in Time-Dependent Density Functional Theory. *Annu. Rev. Phys. Chem.* **2022**, *73*, 117–140, DOI: 10.1146/annurev-physchem-082720-124933.

(22) Gross, E. K.; Oliveira, L. N.; Kohn, W. Rayleigh-Ritz variational principle for ensembles of fractionally occupied states. *Phys. Rev. A* **1988**, *37*, 2805–2808.

(23) Gross, E. K.; Oliveira, L. N.; Kohn, W. Density-functional theory for ensembles of fractionally occupied states. I. Basic formalism. *Phys. Rev. A* **1988**, *37*, 2809–2820.

(24) Gould, T.; Pittalis, S. Hartree and Exchange in Ensemble Density Functional Theory: Avoiding the Nonuniqueness Disaster. *Phys. Rev. Lett.* **2017**, *119*, 1–5, DOI: 10.1103/PhysRevLett.119.243001.

(25) Fromager, E. Individual Correlations in Ensemble Density Functional Theory: State- And Density-Driven Decompositions without Additional Kohn-Sham Systems. *Phys. Rev. Lett.* **2020**, *124*, 243001, DOI: 10.1103/PhysRevLett.124.243001.

(26) Levy, M.; Nagy, A. Variational density-functional theory for an individual excited state. *Phys. Rev. Lett.* **1999**, *83*, 4361–4364.

(27) Nagy, A.; Levy, M. Variational density-functional theory for degenerate excited states. *Phys. Rev. A. At. Mol. Opt. Phys.* **2001**, *63*, 525021–525026, DOI: 10.1103/PhysRevA.63.052502.

(28) Ayers, P. W.; Levy, M.; Nagy, A. Time-independent density-functional theory for excited states of Coulomb systems. *Phys. Rev. A* **2012**, *85*, 042518.

(29) Yang, W.; Ayers, P. W. Foundation for the ΔSCF Approach in Density Functional Theory. *Arxiv* **2024**,

(30) Filatov, M.; Martínez, T. J.; Kim, K. S. Description of ground and excited electronic states by ensemble density functional method with extended active space. *J. Chem. Phys.* **2017**, *147*, 064104.

(31) Lu, Y.; Gao, J. Multistate Density Functional Theory : Theory , Methods , and Applications. *Wiley Interdiscip. Rev. Comput. Mol. Sci.* **2025**, *15*, 1–35, DOI: 10.1002/wcms.70043.

(32) Lu, Y.; Gao, J. Multistate Density Functional Theory of Excited States. *J. Phys. Chem. Lett.* **2022**, *13*, 7762–7769.

(33) Lu, Y.; Zhao, R.; Zhang, J.; Liu, M.; Gao, J. Minimal Active Space: NOSCF and NOSI in Multistate Density Functional Theory. *J. Chem. Theory Comput.* **2022**, *18*, 6407–6420.

(34) Lu, Y.; Gao, J. Function domains and the universal matrix functional of multi-state density functional theory. *J. Chem. Phys.* **2025**, *162*.

(35) Humeniuk, A. Approximate Functionals for Multistate Density Functional Theory. *J. Chem. Theory Comput.* **2024**, *20*, 5497–5509, DOI: 10.1021/acs.jctc.4c00330.

(36) Gao, J.; Lu, Y. Local Spectral Formulation of the One-Determines-All (ODA) Principle

for Multistate Density Functionals. *The Journal of Physical Chemistry Letters* **2026**, *17*, 5639–5645, DOI: 10.1021/acs.jpclett.6c01125, PMID: 42085550.

(37) Gao, J.; Grofe, A.; Ren, H.; Bao, P. Beyond Kohn–Sham approximation: hybrid multistate wave function and density functional theory. *J. Phys. Chem. Lett.* **2016**, *7*, 5143–5149.

(38) Ren, H.; Provorse, M. R.; Bao, P.; Qu, Z.; Gao, J. Multistate Density Functional Theory for Effective Diabatic Electronic Coupling. *J. Phys. Chem. Lett.* **2016**, *7*, 2286–2293, DOI: 10.1021/acs.jpclett.6b00915.

(39) Grofe, A.; Qu, Z.; Truhlar, D. G.; Li, H.; Gao, J. Diabatic-At-Construction Method for Diabatic and Adiabatic Ground and Excited States Based on Multistate Density Functional Theory. *J. Chem. Theory Comput.* **2017**, *13*, 1176–1187, DOI: 10.1021/acs.jctc.6b01176.

(40) Guo, X.; Qu, Z.; Gao, J. The charger transfer electronic coupling in diabatic perspective: A multi-state density functional theory study. *Chem. Phys. Lett.* **2018**, *691*, 91–97, DOI: 10.1016/j.cplett.2017.10.061.

(41) Liu, M.; Chen, X.; Grofe, A.; Gao, J. Diabatic States at Construction (DAC) through Generalized Singular Value Decomposition. *J. Phys. Chem. Lett.* **2018**, *9*, 6038–6046, DOI: 10.1021/acs.jpclett.8b02472.

(42) Bao, P.; Hettich, C. P.; Shi, Q.; Gao, J. Block-Localized Excitation for Excimer Complex and Diabatic Coupling. *J. Chem. Theory Comput.* **2021**, *17*, 240–254, DOI: 10.1021/acs.jctc.0c01015.

(43) Zhao, R.; Grofe, A.; Wang, Z.; Bao, P.; Chen, X.; Liu, W.; Gao, J. Dynamic-then-Static Approach for Core Excitations of Open-Shell Molecules. *J. Phys. Chem. Lett.* **2021**, *12*, 7409–7417, DOI: 10.1021/acs.jpclett.1c02039.

(44) Zhao, R.; Hettich, C. P.; Chen, X. Minimal-active-space multistate density functional theory for excitation energy involving local and charge transfer states. *npj Comput. Mater.* **2021**, *7*, 1–10, DOI: 10.1038/s41524-021-00624-3.

(45) Han, J.; Zhao, R.; Guo, Y.; Qu, Z.; Gao, J. Minimal Active Space for Diradicals Using Multistate Density Functional Theory. *Molecules* **2022**, *17*, 3466.

(46) Liu, C.; Xu, Y.; Bao, P.; Lu, Y. *Adv. Quantum Chem.*; Elsevier, 2025; pp 1–28, DOI: 10.1016/bs.aiq.2025.03.010.

(47) Lu, Y.; Gao, J. Structure of Multi-State Correlation in Electronic Systems. *J. Chem. Theory Comput.* **2024**, *20*, 8474–8481, DOI: 10.1021/acs.jctc.4c00545.

(48) Lu, Y.; Gao, J. Fundamental Variable and Density Representation in Multistate DFT for Excited States. *J. Chem. Theory Comput.* **2022**, *18*, 7403–7411.

(49) Tao, J.; Perdew, J. P.; Staroverov, V. N.; Scuseria, G. E. Climbing the density functional ladder: Nonempirical meta-generalized gradient approximation designed for molecules and solids. *Phys. Rev. Lett.* **2003**, *91*, DOI: 10.1103/PhysRevLett.91.146401.

(50) Cohen, A. J.; Mori-Sanchez, P.; Yang, W. T. Challenges for Density Functional Theory. *Chemical Reviews* **2012**, *112*, 289–320.

(51) Pribram-Jones, A.; Yang, Z. H.; Trail, J. R.; Burke, K.; Needs, R. J.; Ullrich, C. A. Excitations and benchmark ensemble density functional theory for two electrons. *J. Chem. Phys.* **2014**, *140*, 1–13, DOI: 10.1063/1.4872255.

(52) Gunnarsson, O.; Jonson, M.; Lundqvist, B. Descriptions of exchange and correlation effects in inhomogeneous electron systems. *Phys. Rev. B* **1979**, *20*, 3136.

(53) Becke, A. Hartree–Fock exchange energy of an inhomogeneous electron gas. *Int. J. Quantum Chem.* **1983**, *23*, 1915–1922.

(54) Becke, A. D.; Roussel, M. R. Exchange holes in inhomogeneous systems: A coordinate-space model. *Physical Review A* **1989**, *39*, 3761.

(55) McWeeny, R. *Methods of Molecular Quantum Mechanics, second edition*; Academic Press, 1992.

(56) Dirac, P. A. Note on exchange phenomena in the Thomas atom. *Math. Proc. Cambridge* **1930**, *26*, 376–385.

(57) Chachiyo, T. Communication: Simple and accurate uniform electron gas correlation energy for the full range of densities. *J. Chem. Phys.* **2016**, *145*, 021101.

(58) Ceperley, D. M.; Alder, B. J. Ground state of the electron gas by a stochastic method. *Phys. Rev. Lett.* **1980**, *45*, 566–569.

(59) Jacob, C. R.; Reiher, M. Spin in density-functional theory. *Int. J. Quantum Chem.* **2012**, *112*, 3661–3684, DOI: 10.1002/qua.24309.

(60) Paszke, A.; Gross, S.; Massa, F.; Lerer, A.; Bradbury, J.; Chanan, G.; Killeen, T.; Lin, Z.; Gimelshein, N.; Antiga, L. et al. Pytorch: An imperative style, high-performance deep learning library. *Advances in neural information processing systems* **2019**, *32*.

(61) Sun, Q.; Zhang, X.; Banerjee, S.; Bao, P.; Barbry, M.; Blunt, N. S.; Bogdanov, N. A.; Booth, G. H.; Chen, J.; Cui, Z.-H. Recent developments in the PySCF program package. *J. Chem. Phys.* **2020**, *153*, 024109.

(62) Handy, N. C. Multi-root configuration interaction calculations. *Chem. Phys. Lett.* **1980**, *74*, 280–283.

(63) Olsen, J.; Roos, B. O.; Jo/rgensen, P.; Jensen, H. J. A. Determinant based configuration interaction algorithms for complete and restricted configuration interaction spaces. *J. Chem. Phys.* **1988**, *89*, 2185–2192.

(64) Lehtola, S.; Steigemann, C.; Oliveira, M. J.; Marques, M. A. Recent developments in libxc—A comprehensive library of functionals for density functional theory. *SoftwareX* **2018**, *7*, 1–5.

(65) Krylov, A. I. Size-consistent wave functions for bond-breaking: The equation-of-motion spin-flip model. *Chemical Physics Letters* **2001**, *338*, 375–384.

(66) Shiozaki, T.; Győrffy, W.; Celani, P.; Werner, H.-J. Communication: Extended multi-state complete active space second-order perturbation theory: Energy and nuclear gradients. *J. Chem. Phys.* **2011**, *135*.

(67) BAGEL, Brilliantly Advanced General Electronic-structure Library. http://www.nubakery.org under the GNU General Public License. `http://www.nubakery.org`.

(68) Eckert-Maksić, M.; Vazdar, M.; Barbatti, M.; Lischka, H.; Maksić, Z. B. Automerization reaction of cyclobutadiene and its barrier height: An ab initio benchmark multireference average-quadratic coupled cluster study. *J. Chem. Phys.* **2006**, *125*.

(69) Schmerwitz, Y. L. A.; Ivanov, A. V.; Jónsson, E. Ö.; Jónsson, H.; Levi, G. Variational Density Functional Calculations of Excited States: Conical Intersection and Avoided Crossing in Ethylene Bond Twisting. *The Journal of Physical Chemistry Letters* **2022**, *13*, 3990–3999, DOI: `10.1021/acs.jpclett.2c00741`, PMID: 35481754.

(70) Robin, M. B. *Higher Excited States of Polyatomic Molecules - volume III*; Academic Press, Inc., 1985.

(71) Ref. 70, p.214, references in table X.A-I.

(72) Levchenko, S. V.; Krylov, A. I. Equation-of-motion spin-flip coupled-cluster model with single and double substitutions: Theory and application to cyclobutadiene. *J. Chem. Phys.* **2004**, *120*, 175–185.

(73) Priyadarsini, S. S.; Gururangan, K.; Shen, J.; Piecuch, P. The Singlet–Triplet Gap of Cyclobutadiene: The CIPSI-Driven CC(P;Q) Study. *The Journal of Physical Chemistry A* **2025**, *129*, 11749–11780, DOI: 10.1021/acs.jpca.5c07572, PMID: 41364831.

(74) Ref. 68, Table II.

(75) Meurer, A.; Smith, C. P.; Paprocki, M.; Čertík, O.; Kirpichev, S. B.; Rocklin, M.; Kumar, A.; Ivanov, S.; Moore, J. K.; Singh, S. et al. SymPy: symbolic computing in Python. *PeerJ Computer Science* **2017**, *3*, e103, DOI: 10.7717/peerj-cs.103.

(76) Johnson, G. W.; Lapidus, M. L. *The Feynman Integral and Feynman's Operational Calculus*; Oxford University Press, 2000; DOI: 10.1093/oso/9780198535744.001.0001.